



Atmospheric CH₄ and CO₂ enhancements and biomass burning emission ratios derived from satellite observations of the 2015 Indonesian fire plumes

Robert J. Parker^{1,3}, Hartmut Boesch^{1,3}, Martin J. Wooster^{2,3}, David P. Moore^{1,3}, Alex J. Webb¹, David Gaveau⁴, and Daniel Murdiyarso^{4,5}

¹Earth Observation Science, Department of Physics and Astronomy, University of Leicester, Leicester, UK

²King's College London, Department of Geography, London, UK

³NERC National Centre for Earth Observation, UK

⁴Center for International Forestry Research, P.O. Box 0113 BOCBD, Bogor, Indonesia

⁵Department of Geophysics and Meteorology, Bogor Agricultural University, Bogor, Indonesia

Correspondence to: Robert Parker (rjp23@le.ac.uk)

Received: 17 March 2016 – Published in Atmos. Chem. Phys. Discuss.: 21 April 2016

Revised: 23 June 2016 – Accepted: 10 July 2016 – Published: 11 August 2016

Abstract. The 2015–2016 strong El Niño event has had a dramatic impact on the amount of Indonesian biomass burning, with the El Niño-driven drought further desiccating the already-drier-than-normal landscapes that are the result of decades of peatland draining, widespread deforestation, anthropogenically driven forest degradation and previous large fire events. It is expected that the 2015–2016 Indonesian fires will have emitted globally significant quantities of greenhouse gases (GHGs) to the atmosphere, as did previous El Niño-driven fires in the region. The form which the carbon released from the combustion of the vegetation and peat soils takes has a strong bearing on its atmospheric chemistry and climatological impacts. Typically, burning in tropical forests and especially in peatlands is expected to involve a much higher proportion of smouldering combustion than the more flaming-characterised fires that occur in fine-fuel-dominated environments such as grasslands, consequently producing significantly more CH₄ (and CO) per unit of fuel burned. However, currently there have been no aircraft campaigns sampling Indonesian fire plumes, and very few ground-based field campaigns (none during El Niño), so our understanding of the large-scale chemical composition of these extremely significant fire plumes is surprisingly poor compared to, for example, those of southern Africa or the Amazon.

Here, for the first time, we use satellite observations of CH₄ and CO₂ from the Greenhouse gases Observing SATel-

lite (GOSAT) made in large-scale plumes from the 2015 El Niño-driven Indonesian fires to probe aspects of their chemical composition. We demonstrate significant modifications in the concentration of these species in the regional atmosphere around Indonesia, due to the fire emissions.

Using CO and fire radiative power (FRP) data from the Copernicus Atmosphere Service, we identify fire-affected GOSAT soundings and show that peaks in fire activity are followed by subsequent large increases in regional greenhouse gas concentrations. CH₄ is particularly enhanced, due to the dominance of smouldering combustion in peatland fires, with CH₄ total column values typically exceeding 35 ppb above those of background “clean air” soundings. By examining the CH₄ and CO₂ excess concentrations in the fire-affected GOSAT observations, we determine the CH₄ to CO₂ (CH₄/CO₂) fire emission ratio for the entire 2-month period of the most extreme burning (September–October 2015), and also for individual shorter periods where the fire activity temporarily peaks. We demonstrate that the overall CH₄ to CO₂ emission ratio (ER) for fires occurring in Indonesia over this time is 6.2 ppb ppm⁻¹. This is higher than that found over both the Amazon (5.1 ppb ppm⁻¹) and southern Africa (4.4 ppb ppm⁻¹), consistent with the Indonesian fires being characterised by an increased amount of smouldering combustion due to the large amount of organic soil (peat) burning involved. We find the range of our satellite-

derived Indonesian ERs (6.18–13.6 ppb ppm⁻¹) to be relatively closely matched to that of a series of close-to-source, ground-based sampling measurements made on Kalimantan at the height of the fire event (7.53–19.67 ppb ppm⁻¹), although typically the satellite-derived quantities are slightly lower on average. This seems likely because our field sampling mostly intersected smaller-scale peat-burning plumes, whereas the large-scale plumes intersected by the GOSAT Thermal And Near infrared Sensor for carbon Observation – Fourier Transform Spectrometer (TANSO-FTS) footprints would very likely come from burning that was occurring in a mixture of fuels that included peat, tropical forest and already-cleared areas of forest characterised by more fire-prone vegetation types than the natural rainforest biome (e.g. post-fire areas of ferns and scrubland, along with agricultural vegetation).

The ability to determine large-scale ERs from satellite data allows the combustion behaviour of very large regions of burning to be characterised and understood in a way not possible with ground-based studies, and which can be logistically difficult and very costly to consider using aircraft observations. We therefore believe the method demonstrated here provides a further important tool for characterising biomass burning emissions, and that the GHG ERs derived for the first time for these large-scale Indonesian fire plumes during an El Niño event point to more routinely assessing spatiotemporal variations in biomass burning ERs using future satellite missions. These will have more complete spatial sampling than GOSAT and will enable the contributions of these fires to the regional atmospheric chemistry and climate to be better understood.

1 Introduction

The 2015–2016 strong El Niño event, which is ongoing in the tropical Pacific at the time of writing, has had a dramatic impact on the amount of landscape burning occurring across large parts of Indonesia. Landscape fires are commonly used in this environment to clear forest and help manage land for agriculture, but an El Niño-driven drought has further dried out the already human-modified landscapes of Central Kalimantan and south Sumatra. These regions are already more flammable than their natural state due to decades of peatland draining and deforestation, anthropogenically driven forest degradation, as well as the legacy of previous large fire events (Wooster et al., 2012). Even short, localised fire events in these environments can lead to significant greenhouse gas (GHG) emissions, as demonstrated by Gaveau et al. (2014), who report that a 1-week fire event in Riau province (Sumatra) was responsible for emitting 172 ± 59 Tg CO₂ eq., approximately 5–10 % of Indonesia's average annual GHG emissions. The 2015 El Niño-driven fire season in Indonesia is already known to have been far more extensive than in

normal years (Voiland, 2016), and during the last very strong El Niño (1997–1998; the strongest yet on record) massive increases in Indonesian fire activity were similarly recorded (Wooster et al., 1998; Page et al., 2002). Indeed all previous El Niño events, back to the next-strongest event after 1997–1998 (i.e. that of 1982–1983), appear to have produced significant increases in burning over Indonesia, as detailed in Wooster et al. (2012). Whilst the degree of fire activity increase associated with El Niño is possible to gauge using, for example, satellite-derived active fire counts, forest cover change or burned area maps (e.g. Trigg et al., 2006; Langner et al., 2007; Langner and Siegert, 2009; Wooster et al., 2012), what is equally valuable is information on the emissions to the atmosphere resulting from these burns, so that their atmospheric impacts can be more fully determined.

Using satellite-derived estimates of burned area along with assumptions on peatland depths of burn, Page et al. (2002) estimated that the 1997 El Niño-driven Indonesian fires released an amount of carbon (0.81–2.57 Pg) equivalent to between 13 and 40 % of that year's annual global carbon emissions from fossil fuels, contributing to the largest annual increase in atmospheric CO₂ concentration detected since records began in the 1950s (Wang et al., 2013). More recently, van der Werf et al. (2010) have reported similarly anomalous estimates for that year's Indonesian burning, based on related methodologies but different data sets. Anomalies in both inter-annual variability and the atmospheric growth rates of CO₂ and CH₄ continue to be attributed to biomass burning events, including El Niño-driven Indonesian fires (Kasischke and Bruhwiler, 2002; van der Werf et al., 2004; Simmonds et al., 2005). It is possible that the 2015–2016 El Niño-driven Indonesian fires, which, at the time of writing, have largely ceased due to heavy rains (but which may well return in 2016), may ultimately be of a similarly anomalous magnitude to those driven by prior El Niño events. Therefore, there exists a strong interest in both quantifying the amount of fire activity occurring and calculating the overall carbon emissions to the atmosphere that result. Furthermore, the types of biomes being affected are important, because whilst post-fire vegetation regrowth in fire-affected areas does subsequently take up some of the released carbon, areas of burned tropical forest are often replaced by plants holding far less carbon per unit area, and the burning of peat represents an effectively permanent transfer of carbon from the land to the atmosphere (Page et al., 2002). The form in which the carbon is emitted into the atmosphere also has a strong bearing on the emission impacts, with most carbon being released as either the long-lived GHG carbon dioxide, the shorter-lived but much stronger GHG methane, or the air pollutant carbon monoxide (Andreae and Merlet, 2001). Typically, burning in tropical forests and especially in peatlands is expected to involve a much higher proportion of smouldering combustion than the more flaming-characterised combustion that occurs in fine-fuel-dominated environments such as grasslands (Christian et al., 2007; Liu et al., 2014). Hence,

fires in peatlands and tropical forests are expected to produce more CO and CH₄ per unit of fuel burned, with a consequent reduction in the amount of CO₂. However, currently the only information on emission makeup in fires in Indonesian biomes come from relatively few lab-based studies where samples of fuels have been burned in combustion chambers (i.e. Christian et al., 2003; Othman and Latif, 2013; Liu et al., 2014). At present there are no known field-based studies of emission makeup, certainly none conducted during El Niño years where the dry conditions may promote different combustion behaviour than occurs under more normal meteorological and fuel moisture conditions, and none where the constituents of the large-scale plumes that most likely contain the bulk of the emitted gases (and aerosols) are assessed. The latter point is important because whilst ground-based sampling can measure emission makeup close to the source, including in the field under real landscape combustion conditions, such an approach is, by necessity, limited to capturing smoke from individual fire locations, usually from smaller fires. These measurements may not fully represent the emission characteristics of the type of large-scale plumes that may actually be responsible for holding most of the combustion products. Aircraft sampling can provide a means to capture the latter's characteristics (e.g. Yokelson et al., 1999), but such campaigns are costly, infrequent and logistically challenging. An alternative approach to characterising the emission makeup of large-scale fire plumes is via satellite-based sounding of wildfire plume chemistry, which has so far been demonstrated only a few times, by Coheur et al. (2009) using IASI onboard MetOp and by Ross et al. (2013) using the TANSO-FTS instrument onboard the Greenhouse gases Observing SATellite (GOSAT). Here, we build on the latter work to exploit GOSAT's observations of CH₄ and CO₂ over the 2015 El Niño-driven Indonesian fires, using these to demonstrate the increase in atmospheric concentrations of CH₄ and CO₂ associated with the large-scale biomass burning plumes, and deriving from these observations the CH₄ to CO₂ emission ratios (ERs) for these El Niño-driven Indonesian fires for the first time. We compare these Indonesian fire emission ratios to those derived from GOSAT in alternative tropical biomes having different combustion characteristics (southern African savannah and the Amazon basin). In combination with fire radiative power (FRP) and atmospheric carbon monoxide data taken from the new Copernicus Atmosphere Service Global Fire Assimilation System (CAMSGFAS, 2016), we demonstrate the Indonesian fires are occurring in peatland-dominated landscapes that explain certain characteristics of the noted ERs, which are themselves important in determining the so-called emission factors representative of the combustion processes occurring in these very large-scale landscape fires.

Emission factors (EFs) are necessary when converting estimates of the amount of fuel burned (obtained from burned area or FRP-based methods) into a quantity of each trace gas (Koppmann et al., 2005; Reid et al., 2005). These EFs are

themselves often calculated through the use of ERs which are determined from the ratio of the excess concentrations emitted from wildfires (Andreae and Merlet, 2001). Whilst the emission factors are only one aspect of calculating the overall emitted amounts, due to the fact that satellite observations of burned area and FRP have significantly improved in recent years, the accuracy of the emission factors is becoming more crucial to the overall accuracy of the emissions (Van Leeuwen and Van Der Werf, 2011). The capability to measure the CH₄ to CO₂ (CH₄ / CO₂) ERs from a variety of wildfires in different biomes across the globe, consistently using a single instrument and/or approach and from very large-scale plumes that represent some of the largest individual fires emission sources, is therefore a significant advancement. We first demonstrated this capability in Ross et al. (2013), and here we focus on extending this determination of satellite-derived CH₄ / CO₂ ERs to Indonesia during the anomalously large El Niño-driven fire season of September–October 2015. The emission ratios themselves are of clear interest in helping to determine the relative amounts of these two key GHGs released by the fires, but also the relative amounts of CH₄ and CO₂ being released in a smoke plume are known to vary with the dominance of smouldering and flaming combustion of the causal fire, as do the more commonly used CO₂ and CO measures (e.g. Lobert and War-natz, 1993; Yokelson et al., 1996; Wooster et al., 2011). Furthermore, knowledge of the relative amounts of these two phases of combustion are known to exert strong controls on the relative emissions of many other compounds (e.g. Yokelson et al., 1996; Cofer et al., 1998; Lee et al., 2010), and thus, if we can better understand the relative CO₂ and CH₄ emission makeup of the large-scale plumes emanating from these fires, it may provide useful information to better estimate the type of combustion occurring and thus potentially the overall emission characteristics beyond the two species observed.

2 El Niño and Indonesian fire activity

El Niño describes a large-scale climate anomaly that typically occurs once or twice per decade, with one of the key characteristics being significantly warmer than normal sea surface temperatures (SSTs) in the equatorial eastern Pacific Ocean (Trenberth, 1997). The many other effects associated with an El Niño event are complex and not always consistent between different El Niños, but most events are accompanied by warmer temperatures across much of South America, Africa, Southeast Asia and western Europe, decreased precipitation over central/southern Africa, central America, Southeast Asia and increased precipitation over the southern United States and western Europe (Hartmann et al., 2013). Indonesia is located in the equatorial region and can be particularly affected by El Niño events, for example, usually experiencing warmer temperatures and significant reductions in rainfall that exacerbate certain aspects of a landscape already

heavily modified by human actions. In particular, much of the low-lying land on the Indonesian islands of Sumatra and Kalimantan that was originally covered by moist, forested peatlands has been cleared and drained for agriculture, and this has led to much drier landscape conditions. Fire is commonly used to manage the land, and during the droughts associated with El Niño, the already heavily disturbed peatland landscapes can become so dry that they can be ignited from the vegetation fires that are widespread even in normal years (Gaveau et al., 2014). Such fires can burn down into the carbon-rich peat for weeks, whilst also spreading across the landscape to ignite new areas – including spreading into areas of remaining tropical forest that normally are not prone to fire. During El Niño these peat and forest fires can thus affect areas that are very much larger than those burned during normal years, particularly during the strongest El Niño events when fire activity can be more than an order of magnitude higher (van der Werf et al., 2008; Wooster et al., 2012). As described in Sect. 1, during the 1997–1998 El Niño, fires in Indonesia are estimated to have released huge amounts of carbon into the atmosphere and because of the smouldering nature of peat (and to some extent, tropical forest as well), a greater proportion of these emissions is likely to be in the form of non-CO₂ gases, primarily the air pollutant CO and the strong greenhouse gas CH₄, than is the case for flaming fires (Christian et al., 2003, 2007). This contrasts with the burning of the El Niño-dried finer fuels, which will typically burn primarily via flaming combustion and thus release a lower proportion of CO and CH₄ and a higher proportion of CO₂, whose global warming potential is significantly lower than that of methane (Myhre et al., 2013). It is estimated that approximately three-fourths of the fire activity over this time period was due to peatland burning (Huijnen et al., 2016).

2.1 Magnitude of El Niño events and the associated fire activity

There are many different ways to quantify the magnitude of an El Niño event but one of the most widely accepted is the Multivariate ENSO Index (MEI) (Wolter and Timlin, 1998). This is based on observations of a variety of meteorological parameters over the tropical Pacific Ocean. By this metric (Wolter, 2016), the current El Niño event that we are experiencing (2015–2016) is already the third strongest event on record (behind 1997–1998 and 1982–1983), with the potential to be classified even higher before it is complete.

To investigate the magnitude of the increased fire activity over Indonesia that has been associated with the current El Niño we examined the fire radiative power being released from the identified combustion zones. FRP is a measure of a fire's release rate of thermal radiation, and is strongly related to the rate of fuel consumption, and trace gas and aerosol emission (Wooster et al., 2005; Freeborn et al., 2008). FRP is therefore both an indicator for the presence of fire, and an estimator for the amount of material being emitted to the at-

mosphere from that fire. Global satellite observations of FRP are made from the MODIS instruments onboard the NASA Terra and Aqua satellites at a nadir spatial resolution of 1 km, and these are incorporated into the Copernicus Atmosphere Monitoring Services (CAMS) Global Fire Assimilation System (GFAS), set up under the Monitoring Atmospheric Composition and Climate (MACC) series of research projects (CAMS-GFAS, 2016). Using FRP data converted to FRP density by dividing by the grid cell area ($0.1^\circ \times 0.1^\circ$) and adjusting for the impact of unseen parts of the land surface due to gaps in satellite coverage and variations in cloud cover (Kaiser et al., 2012), GFAS produces estimates of trace gas emissions from the mapped fire-affected areas, which CAMS then uses in its atmospheric chemistry transport model to identify atmospheric abundances of the released chemical species.

Figure 1 shows the monthly total FRP density (in W m^{-2}) over the Indonesian region (defined as 5°N – 10°S , 90 – 150°E) for the last 7 years, calculated from the GFAS data, including adjustments for observation frequency and cloud cover (Kaiser et al., 2012). Whilst significant landscape burning takes place every year between July and October in this Indonesian region, the fires that took place in the latter part of 2015 (particularly September and October 2015) were clearly of an extreme magnitude, with the cumulative FRP density for October 2015 exceeding 7500 W m^{-2} , compared to the second-highest value of just over 2000 W m^{-2} (October 2014).

Whilst FRP gives an indication of the intensity of fires and their associated emissions to the atmosphere, the number of fires is also a useful indicator of fire activity, especially in regions which may see many small fires as opposed to fewer, but larger, events (Wooster and Zhang, 2004; Schroeder et al., 2014). For this reason, the original MODIS MOD14/MYD14 fire counts were also examined (Giglio et al., 2003). The number of fires observed by MODIS across Indonesia during September–October 2015 is shown in Fig. 2. Overlain onto this in green are the locations of known peatlands in Sumatra, Kalimantan and Papua (Ritung et al., 2016). It is clear that the majority of the most fire-affected regions of Indonesia during the September and October extreme fire event, i.e. Central Kalimantan and the southeastern region of Sumatra, are located in areas dominated by peatlands.

2.2 Fire emissions and combustion regimes

As already stated, in contrast to the flaming combustion involved in the burning of wood and/or grass, peatland fires are typically dominated by deeper smouldering combustion. As smouldering combustion is less efficient than flaming combustion, there is a higher proportion of CO, CH₄ and other non-methane hydrocarbons (NHMCs) released compared to CO₂ (Bertschi et al., 2003; Yokelson et al., 2008; Wooster et al., 2011).

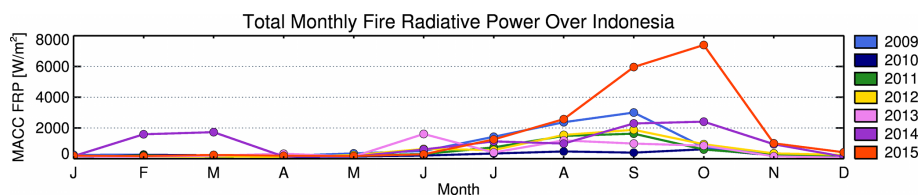


Figure 1. Time series of the monthly total fire radiative power density (W m^{-2}) recorded over the Indonesian region (defined as 5°N – 10°S , 90 – 150°E) between 2009 and 2015, calculated using data from the CAMS Global Fire Assimilation System (Kaiser et al., 2012). September and October 2015 are clearly anomalous compared to the previous years shown, highlighting the effect of this year's El Niño on the region's fire activity.

A literature review of previous ground- and aircraft-based measurements of the CH_4/CO_2 ER indicates a wide range of values, demonstrating the variability that can be dependent on not only the fuel type but also on additional factors, such as fuel moisture content, the ratio of living to dead matter and how recently the area last burned (Korontzi et al., 2003). To take just one example, Koppmann et al. (1997) present CH_4/CO_2 ER values for flaming fires of 2.6 ppb ppm^{-1} from sugar cane fields, increasing to 10.3 ppb ppm^{-1} over fires dominated by smouldering combustion in forest and shrubland. Fires with intermediate values were reported to represent a mixture of smouldering and flaming combustion. Similarly, Hurst et al. (1994) report mean ER values of $2.1 \pm 1.5\text{ ppb ppm}^{-1}$ for flaming combustion, $5.3 \pm 2.0\text{ ppb ppm}^{-1}$ for mixed combustion and $10.1 \pm 3.9\text{ ppb ppm}^{-1}$ for smouldering combustion. A further study (Bonsang et al., 1995) presents values of 3.2 – 4.6 ppb ppm^{-1} for flaming combustion, increasing to 7.8 ppb ppm^{-1} for smouldering combustion in savannah or forest regions. The wide range of CH_4 to CO_2 ERs reported by these different studies demonstrates that, even when measured close to the source, as all these were, there is a high degree of variability intrinsic to the CH_4/CO_2 ER but the relative behaviour remains consistent, namely that flaming processes produce smoke with a lower CH_4 to CO_2 ratio than smouldering processes, and thus it may be possible to distinguish between these two types of combustion using measurements of this ratio.

The objectives of this work are to first determine whether the expected high concentrations of CH_4 emitted by the extreme peatland burning in September–October 2015 over Indonesia are observable from satellite data and, if that is the case, to then determine the CH_4/CO_2 ER of the resulting large-scale smoke plumes and compare this to measurements made in situ. The capability to examine the large-scale ERs of a region such as this is important because if GOSAT can measure CH_4/CO_2 ERs, such observations contain information related to the mix of combustion types occurring and can thus help discriminate predominantly smouldering from predominantly flaming regions. Not only is this of direct interest for the CH_4 and CO_2 emissions themselves but is also useful when considering the many other species contained within

the smoke, because the relative abundance of most of these is in part dependent on the amount of flaming and smouldering combustion occurring.

This work is presented as follows. Section 3 introduces the GOSAT satellite data used in this work, providing details on the retrieval method and how the CH_4/CO_2 data have been used to determine fire ERs. Section 4 describes the methodology used for determining whether a GOSAT sounding is affected by fire and provides statistics on the number of fire-affected soundings that we observe over the Indonesian fire region. Section 5 goes on to examine the enhancement in CH_4 as observed from the fire-affected data while Sect. 6 then uses these data to determine CH_4/CO_2 fire ERs, comparing them to in situ observations of the same El Niño-driven fire event. Finally, we summarise our findings and comment on the outlook for further study in this area of research.

3 GOSAT Proxy XCH_4 data

GOSAT was the first dedicated greenhouse gas measurement mission based on an Earth observation satellite approach, and was launched by the Japanese Space Agency (JAXA) on 23 January 2009 (Kuze et al., 2009). GOSAT is equipped with two instruments. The first is the Thermal And Near infrared Sensor for carbon Observation – Fourier Transform Spectrometer (TANSO-FTS), which provides point-based measurements of total column CO_2 and CH_4 with near-surface sensitivity because of its use of a shortwave infrared (SWIR) as well as a thermal infrared (TIR) band sensitive to the mid-troposphere. The second is the Cloud and Aerosol Imager (TANSO-CAI), which provides multispectral imagery at 0.5 km resolution with bands at 0.38 , 0.67 , 0.87 and $1.6\text{ }\mu\text{m}$. This allows additional cloud–aerosol information about the region of interest within which the TANSO-FTS measurement footprints fall.

The TANSO-FTS measurement pattern originally consisted of five (later changed to three) across-track points with a footprint of $\sim 10.5\text{ km}$, each separated by approximately 100 km on the ground. GOSAT also has capabilities for agile pointing, allowing both target mode and observations of the glint spot over the ocean. Near-surface sensitiv-

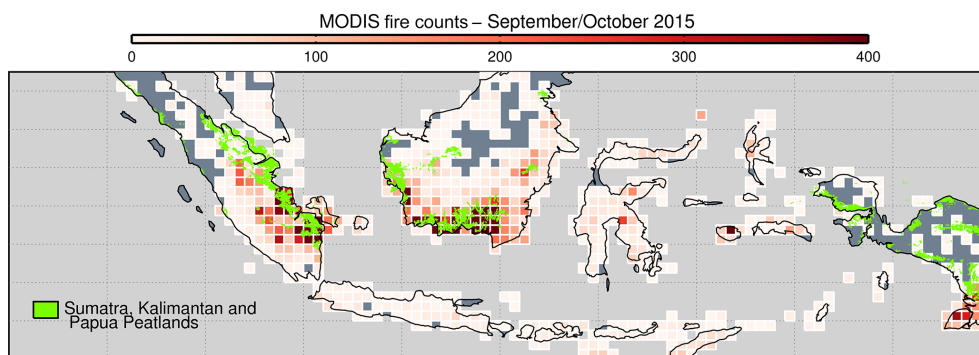


Figure 2. MODIS fire counts for September–October 2015 over the Indonesia, gridded into $0.5^\circ \times 0.5^\circ$ boxes. Also overlaid are the locations of known peatlands in Sumatra (left), Kalimantan (centre) and Papua (right).

ity to the target gases is achieved by the TANSO-FTS instrument utilising three SWIR spectral bands at 0.76, 1.6 and $2.0\ \mu\text{m}$, with mid-tropospheric sensitivity available from a fourth band operating between 5.5 and $14.3\ \mu\text{m}$ in the TIR. Kuze et al. (2016) provide extensive details of the performance and operation of the TANSO-FTS instrument over the past 6 years. In short, although GOSAT has experienced three major anomalies over its lifetime (a solar paddle failure in May 2014, a pointing system issue in January 2015 and a cryocooler restart in September 2015), it continues to operate well, providing high-quality atmospheric radiance measurements from which we are able to retrieve dry-air, column-averaged fractions of CO_2 and CH_4 (denoted as XCO_2 and XCH_4 , respectively).

Details of the University of Leicester Proxy XCH_4 GOSAT retrieval, including recent updates and uncertainty characterisation, can be found in Parker et al. (2011, 2015). In brief, the retrieval utilises the original Orbiting Carbon Observatory (OCO) so-called full-physics retrieval algorithm (as the radiative transfer attempts to explicitly model the physical behaviour of the aerosol-scattered light) (Boesch et al., 2011; Cogan et al., 2012; O'Dell et al., 2012) developed to obtain XCO_2 from a simultaneous fit of NIR/SWIR O_2 and CO_2 bands, and subsequently modified to operate on GOSAT spectral data to retrieve XCH_4 using the light-path Proxy approach. Developed by Frankenberg et al. (2006) for use on SCIAMACHY data, this Proxy method utilises the fact that the majority of the influence of atmospheric scattering on the retrieved XCH_4 can be negated through the co-retrieval of the spectrally close $1.6\ \mu\text{m}$ CO_2 band, since the signal related to both species undergoes the same light-path enhancement through scattering. The resulting $\text{XCH}_4 / \text{XCO}_2$ ratio is therefore robust to the effects of aerosol. Generally the final Proxy XCH_4 is obtained via the application of XCO_2 model fields to this ratio. Typically, due to the fact that there is significantly less influence from aerosol on the final product than with the typical full-physics retrieval approach (Butz et al., 2010), high-quality retrievals are possible even under cloud–aerosol conditions where the

typical full-physics retrieval struggles. Not only does this result in many more successful soundings globally but it also allows studies over cloudy or smoke-affected regions where no data at all may be available from the typical full-physics retrieval approach.

XCH_4 data obtained using the Proxy approach described above have been used in many inversion studies (Fraser et al., 2013; Wecht et al., 2014; Fraser et al., 2014; Cressot et al., 2014; Alexe et al., 2015; Turner et al., 2015) to estimate both global and regional emissions of XCH_4 . Normally the main disadvantage of the Proxy XCH_4 retrieval is that it requires an accurate and unbiased XCO_2 model to convert the ratio back into XCH_4 (Schepers et al., 2012). However, in our current study of the atmospheric impacts and ERs of the El Niño-driven fires in Indonesia, we use only the individual retrieved XCH_4 and XCO_2 components of the Proxy retrieval and hence, we have no dependence on any CO_2 model. For the purposes of this study, the standard GOSAT Proxy data record (typically generated as part of the ESA GHG-CCI project (Buchwitz et al., 2015), 4–6 months behind real time due to the use of ECMWF ERA-Interim data in the processing chain) has been extended with the use of ECMWF Analysis data in order to produce results more quickly than possible with the normal route. In this way, the Proxy XCH_4 time series has been extended from June to November 2015 and includes retrievals both over land and also over ocean when GOSAT measures in a sun-glint geometry.

In Sect. 1, it was shown that September–October 2015 exhibited significantly higher FRP over Indonesia than previous years. Before exploring the GOSAT data over Indonesia in more detail, it is first useful to put the GHG observations for September and October 2015 into the context of the longer GOSAT time series. Figure 3 shows the 95th percentile values for the monthly GOSAT data over Indonesia for the entire data record from April 2009 to November 2015. The upper panel shows the $\text{XCH}_4 / \text{XCO}_2$ ratio, with the central and lower panels showing the individual XCH_4 and XCO_2 , respectively.

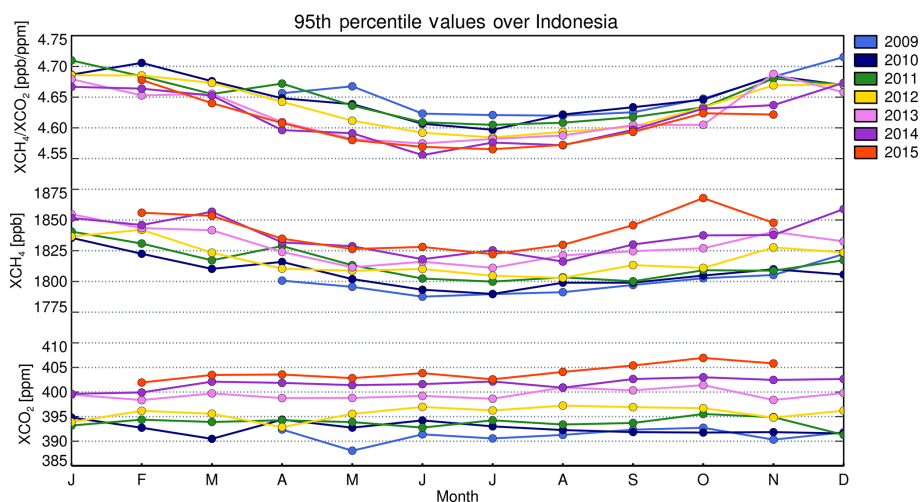


Figure 3. Time series showing the monthly 95th percentile values over Indonesia for the GOSAT Proxy XCH_4 / XCO_2 (top) as well as the individual XCH_4 (middle) and XCO_2 (bottom) components of the Proxy data for the entire GOSAT data record (2009–present).

In order to quantify the extreme nature of the October 2015 observations and to account for the annual growth rate, we define the magnitude of the enhancement as the October–July difference for each year, with July typically signifying the start of the fire season in this region. For CO_2 , we observe a magnitude of 4.35 ppm for October 2015 compared to a mean value of 1.05 ± 1.42 ppm for the previous years (2009–2014). In the case of XCH_4 , the enhancement value for October 2015 is found to be 45.65 ppb compared to an average for previous years of 11.93 ± 3.60 ppb. The enhancement of both the XCO_2 and, in particular, XCH_4 in October 2015 is therefore significantly higher than that observed over the region in previous years, corresponding to the extreme in fire activity observed in Fig. 1.

4 Identifying fire-affected GOSAT soundings

Section 3 established that a significant increase is observed in the monthly maximum values for the XCH_4 , XCO_2 and the XCH_4 / XCO_2 during September–October 2015 (calculated as the 95th percentile values) recorded over Indonesia by GOSAT. To further investigate the atmospheric GHG anomalies identified over Indonesia by GOSAT in Fig. 3, it is first necessary to identify which GOSAT soundings are directly affected by fire emissions, and which can be considered background (clear) cases.

We use the CAMS CO fields to determine if a particular GOSAT sounding is likely to be fire affected. In addition to emissions from CO sources and their atmospheric transport, the CAMS CO fields incorporate carbon monoxide total column measurements from the IASI and MOPITT instruments (Inness et al., 2015). We sampled the CO fields at the time and location of each GOSAT sounding, and based on the CO distribution and data from the GOSAT CAI, values in excess

of 0.003 kg m^{-2} were determined as being likely affected by the local fire emissions. Conversely, if the CO value was less than $0.00075 \text{ kg m}^{-2}$ then the sounding was classed as clear (i.e. unaffected by local fire emissions). GOSAT soundings corresponding to locations and times having CO values between these thresholds were not able to be confidently classed as either fire affected or clear. Out of 3946 GOSAT soundings over Indonesia during September–October 2015, the CAMS CO identified 341 (8.6%) of these as being affected by fire and 1272 (32.3%) as clear (i.e. unaffected by fire), with the remainder lying between these thresholds.

Figure 4 shows a GOSAT CAI false-colour image covering much of Kalimantan on 21 October 2015, a time when a massive pall of smoke enveloped Central Kalimantan and parts of the surrounding regions. The active fire detections for this day made from MODIS are also shown (small purple circles), along with the numbered locations of the individual GOSAT TANSO-FTS soundings (red circles). All GOSAT soundings made coincident with this CAI image were in locations where the simultaneous CAMS CO field indicated the corresponding TANSO-FTS measurement was fire affected.

5 Observations of enhanced methane concentrations

Once we had identified a set of GOSAT soundings that were able to be clearly classed as fire affected or clear, it became possible to examine the XCH_4 , XCO_2 and XCH_4 / XCO_2 distributions in order to determine the changes in the column amount and trace gas ratio characteristics related to the extreme levels of fire activity. Figure 5 shows histograms of the XCH_4 / XCO_2 ratio, as well as the individual XCH_4 and XCO_2 components, for all the clear (blue) and fire-affected (red) soundings, as well as for the entire data set (green).

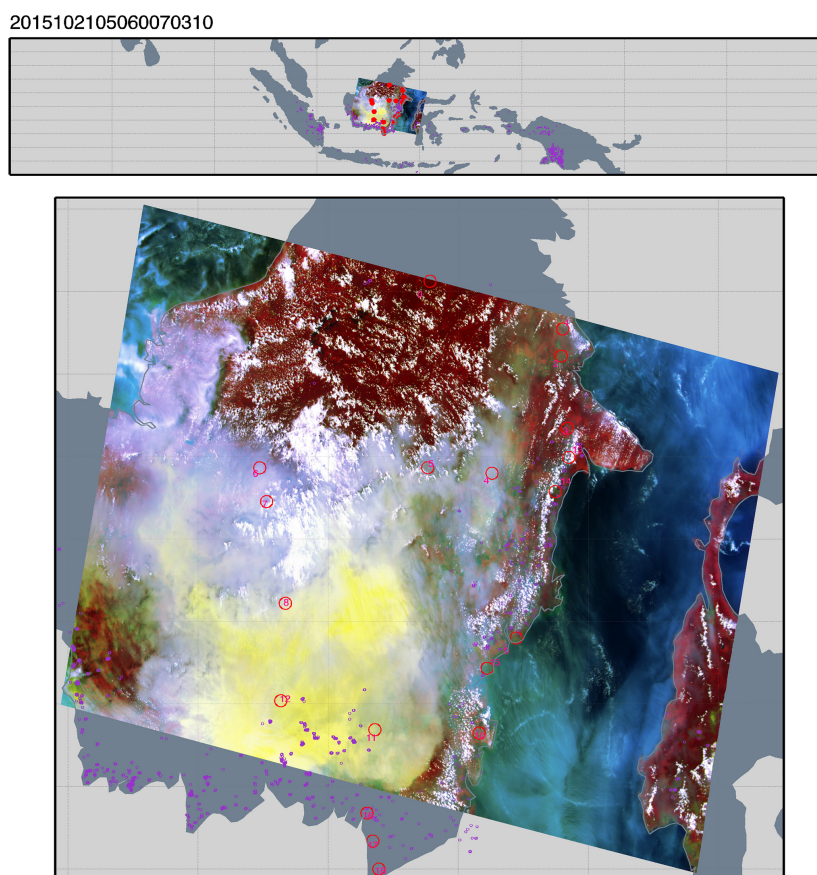


Figure 4. False-colour image (RGB indicates CAI band 3, 2, 1) derived from data taken by the GOSAT CAI, collected when the GOSAT satellite passed over the island of Borneo on 21 October 2015 (around 13:00 LT, 05:00 UTC), a period when extreme fires were burning across much of Central Kalimantan. GOSAT TANSO-FTS sounding locations are identified by the numbered large red circles, with the MODIS active fire detections identified by the small purple circles.

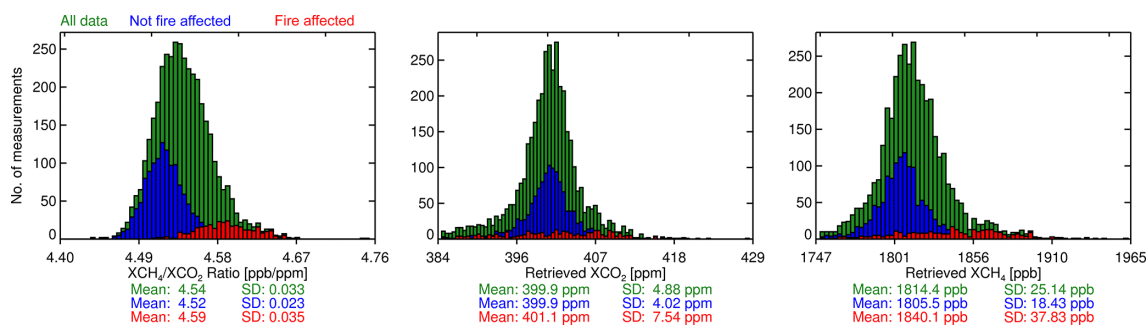


Figure 5. Histograms showing the distributions over Indonesia in September–October 2015 of the XCH₄ / XCO₂ ratio (left), the retrieved XCO₂ (centre) and the retrieved XCH₄ (right) for all data (green), data determined to be definitely affected by fire emissions (red) and those classed as clear (blue). Also included are the corresponding mean and standard deviation values for each distribution.

As Table 1 shows, for the XCH₄ / XCO₂ ratio, the mean ratio calculated from all the data is 4.54 ppb ppm⁻¹, with a standard deviation of 0.033 ppb ppm⁻¹. The histograms for the clear and fire-affected data show two clearly separated distributions, with means of 4.52 and 4.59 ppb ppm⁻¹, respectively. When examining just the XCO₂ distributions,

there appears to be less of a distinct separation, with means of 399.9 and 401.1 ppm, respectively, for the clear and fire-affected cases. This corresponds to a XCO₂ increase of 0.3 % percent over the background XCO₂ concentrations, whereas the XCH₄ distribution for the fire-affected scenes shows a

Table 1. Table showing the mean and standard deviation over Indonesia in September–October 2015 of the XCH_4 / XCO_2 ratio (left), the retrieved XCO_2 (centre) and the retrieved XCH_4 (right) for all data, data determined to be unaffected by fire and data determined to be affected by fire.

	XCH_4 / XCO_2 (ppb ppm ⁻¹)		XCO_2 (ppm)		XCH_4 (ppb)	
	Mean	SD	Mean	SD	Mean	SD
All	4.54	0.033	399.9	4.88	1814.4	25.14
Clear	4.52	0.023	399.9	4.02	1805.5	18.43
Fire affected	4.59	0.035	401.1	7.54	1840.1	37.83

much larger mean enhancement of 1.9% percent over the background (1840.1 ppb vs. 1805.5 ppb).

In order to examine the spatial distribution of the atmospheric GHGs and XCH_4 / XCO_2 ratio enhancements, Fig. 6 shows (top to bottom) maps of the GOSAT-retrieved XCH_4 , XCO_2 , XCH_4 / XCO_2 ratio, along with the CAMS total column CO and IASI total column CO for all TANSO-FTS sounding locations (left), clear locations (centre) and fire-affected locations (right). These data show that the spatial extent of the enhancements in XCH_4 , XCO_2 and in the resulting XCH_4 / XCO_2 ratio, as well as in the CAMS and IASI CO, are related to the enhanced fire activity seen over parts of Sumatra and Kalimantan (shown in Fig. 2), whose emissions are being transported primarily westwards over the ocean (last column of Fig. 6).

This finding confirms that the anomalously large amount of fire activity seen occurring in September and October 2015 during the El Niño (Fig. 1) and which included fires in the extensive peatlands of Central Kalimantan and south Sumatra (Fig. 2) resulted in a significant increase in atmospheric column amounts of CH_4 and CO_2 downwind of the fires. These enhancements are observable from GOSAT satellite observations, and in the following section we examine the CH_4 / CO_2 ER of this smoke to better understand the combustion characteristics.

6 Determination of CH_4 / CO_2 ERs

As discussed in Sect. 2, the capability to determine large-scale regional ERs during intense fire activity is important, as it allows information to be gained not only on the emissions of these gases themselves but also potentially on the relative dominance of flaming vs. smouldering combustion. Our previous work, Ross et al. (2013), demonstrated for the first time an ability to determine CH_4 / CO_2 fire ERs from satellite data, in that case using GOSAT to study ERs of boreal forest (Canada and Russia), tropical forest (Brazil) and savannah (southern Africa) fires. The satellite-derived ERs obtained appeared to be in good agreement with those derived during ground and aircraft sampling studies in the same biomes, albeit these in situ data themselves show relatively large variations. Such variability is likely a function of differences in

fuel type, fuel moisture and fire behaviour that occurred between different measurement campaigns, fire locations and time of year or day (Van Leeuwen and Van Der Werf, 2011). Here, we apply the technique of Ross et al. (2013) to our current GOSAT Proxy retrievals of XCO_2 and XCH_4 made during the September–October 2015 Indonesian fires, in order to determine the ERs characterising the very large-scale plumes seen during this anomalously large climate-related fire event.

As a first step in this process, it is useful to calculate the excess (or Δ) XCH_4 and XCO_2 values prior to any subsequent processing, since, for example, the fire emissions can be superimposed into a background atmosphere that itself contains spatially and/or temporally varying amounts of XCH_4 and XCO_2 . Calculating such excess amounts removes the impact of potentially varying background concentrations. However, since we utilise the XCH_4 and XCO_2 components of the GOSAT Proxy XCH_4 retrieval, which themselves do not account explicitly for aerosol scattering (but instead rely on these effects to ratio out when computing the final Proxy XCH_4 values; see Sect. 3), this does provide some potential for error to be introduced in any subsequently calculated CH_4 / CO_2 emission ratio. Such errors are related to the fact that the degree of scattering may be different between the fire-affected (i.e. smoke-laden) and matching background (i.e. clear) TANSO-FTS soundings from which the excess amounts are calculated. We analysed the magnitude of this effect using a simple model, included in Appendix A, and the results indicate that it is possible to underestimate the CH_4 / CO_2 ER by $\sim 10\%$ if appropriate care is not taken during selection of the clear soundings whose column amounts are to be subtracted from those of the fire-affected soundings in order to calculate the excess column amounts. In a region such as Indonesia during El Niño, where large-scale fire activity is clearly greatly affecting the aerosol composition of the local atmosphere, this aspect becomes even more challenging. To deal with this, we only used fire-affected TANSO-FTS soundings made over land, so as to minimise the effect of mixing and/or dilution as smoke-laden air was transported longer distances over the ocean. For each fire-affected sounding, a matching background measurement was selected from the group of clear soundings located over the same island and as close as possible to the fire-affected measurement (e.g. the background for the Sumatra soundings

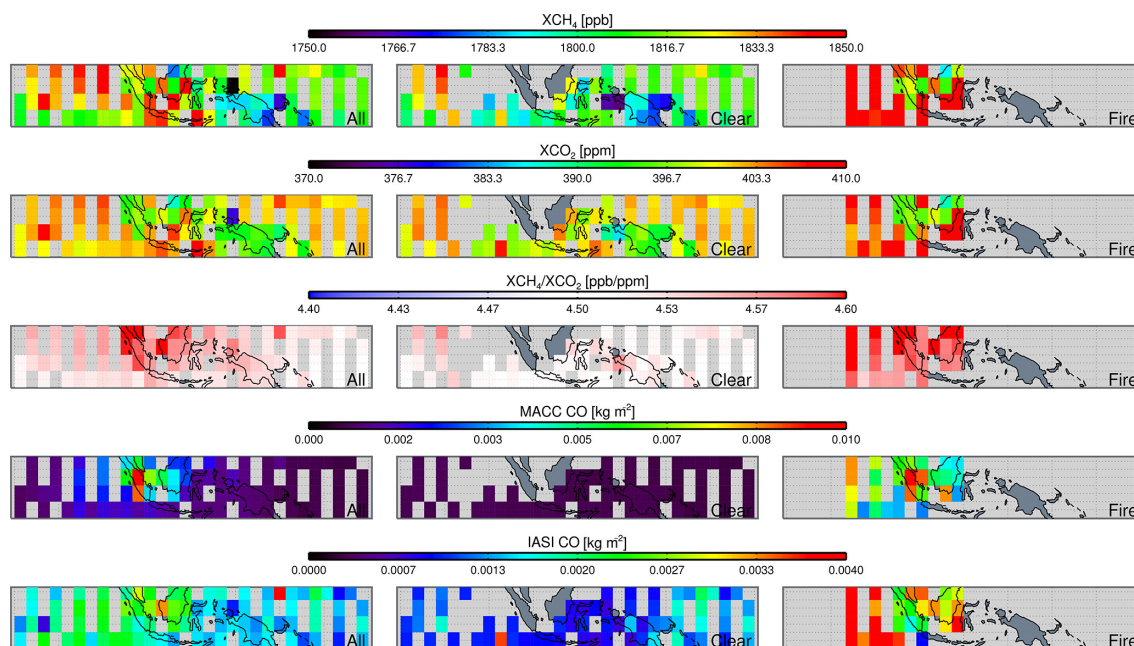


Figure 6. Indonesia trace gas distributions for September–October 2015 showing (top to bottom): the GOSAT-retrieved XCH_4 , XCO_2 and XCH_4 / XCO_2 ratio, along with the CAMS carbon monoxide (CO) total column and the measured IASI CO total column. The left column shows all data gridded at $2^\circ \times 2^\circ$, the central column shows only those points determined to be clear using the criteria of Sect. 4 and the right column shows the data determined to be fire affected based on the same criteria.

were selected from clear soundings between $90\text{--}108^\circ \text{E}$ and $5^\circ \text{N--}10^\circ \text{S}$) in order to minimise impacts stemming from use of non-uniform background measurements as detailed in Yokelson et al. (2013). Out of 131 fire-affected soundings, a suitable background sounding was identified for 105 (80 %) of the soundings. Each background XCH_4 and XCO_2 value was then subtracted from the concentration derived from its corresponding fire-affected sounding in order to produce the ΔXCH_4 and ΔXCO_2 values, from which the ERs could then be calculated.

Figure 7 shows the ΔXCH_4 values plotted against the simultaneously derived ΔXCO_2 values for all of the fire-affected soundings measured over Indonesia for the September–October 2015 period. The CH_4 / CO_2 ER derived from the linear best fit to these data is 6.2 ppb ppm^{-1} (correlation coefficient of 0.937). Whilst this calculated CH_4 / CO_2 ER is significantly above that of the ambient background ($\sim 4.52 \text{ ppb ppm}^{-1}$), the many fire plumes sampled by GOSAT soundings across the September–October 2015 period mean that potential variations in the emission ratios over time (and space) can also be explored. Figure 8 once again shows the daily CAMS FRP density data, but this time for September–October 2015 only, and as a daily average for the entire Indonesian region as well as for Sumatra and Kalimantan individually. There is very significant variability seen in the fire activity across these 2 months, and we identify several distinct time periods to examine in more detail for both Sumatra and Kalimantan. The period 9–15 September over

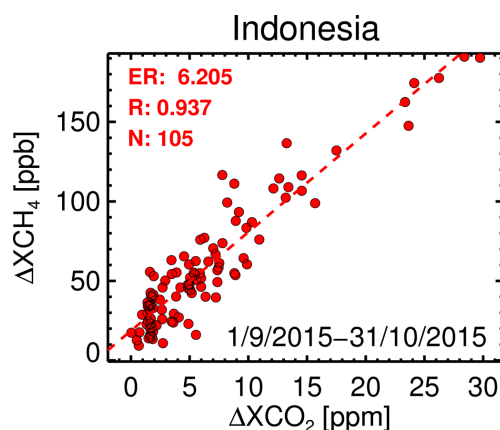


Figure 7. Scatterplot of GOSAT-derived ΔXCH_4 vs. ΔXCO_2 values for large-scale fire plumes seen over Indonesian region (of the type seen in Fig. 4) from 1 September to 31 October 2015, calculated as the total column difference between the fire-affected and corresponding clear background TANSO-FTS soundings. The CH_4 / CO_2 ER, (ppb ppm^{-1}) is calculated from the gradient of a linear best fit, shown as the dashed line. Also shown are the correlation coefficient R and the number of soundings N .

Sumatra is characterised by a steady increase in FRP density, peaking on 12 September at over 200 W m^{-2} before decreasing again and reducing to below 50 W m^{-2} by 15 September. We take this as Period 1 for Sumatra. By contrast, over Kalimantan at around the same time (specifically between the 8

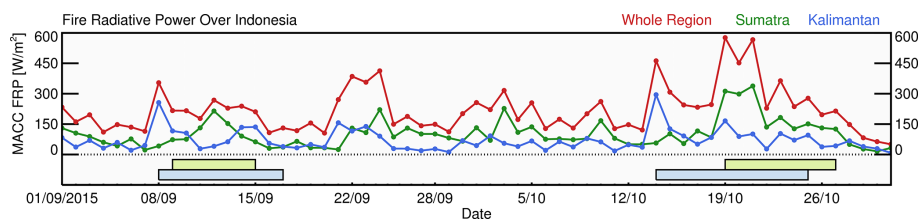


Figure 8. Daily fire radiative power density (red line) taken from the Global Fire Assimilation System (GFAS) (Kaiser et al., 2012), operated as part of CAMS. Data are shown from 1 September to 31 October 2015, for the entire Indonesian landmass (red) and separately for the regions of Sumatra and Kalimantan. Two specific time periods are highlighted (referred to as Period 1 and Period 2), Period 1 covering 9–15 September (Sumatra) and 8–17 September (Kalimantan) and Period 2 covering 19–27 October (Sumatra) and 14–25 October (Kalimantan).

and 17 September) there is a peak in FRP on 8 September of nearly 300 W m^{-2} , followed by a lull around the middle period before a second increase to almost 150 W m^{-2} on 13–14 September. We take this as Period 1 for Kalimantan. In contrast to the differing behaviours during Period 1, both Sumatra and Kalimantan exhibit somewhat more similar trends in fire activity during Period 2, starting with a high peak (over 300 W m^{-2}) on 19 and 14 October for Sumatra and Kalimantan, respectively, however, while over Kalimantan the fire activity then immediately reduced to a lower level (around 100 W m^{-2}). Over Sumatra, high FRP density values in excess of 300 W m^{-2} are maintained over several days before slowly decreasing. This suggests a significantly larger fire event over Sumatra than over Kalimantan at this time, a finding consistent with the CAMS total column CO fields (e.g. as seen in Fig. 6). Although Fig. 8 suggests that an additional period centred around 22 September should be of interest, there are insufficient GOSAT soundings during this time from which to determine an ER, demonstrating that the somewhat limited GOSAT sampling strategy can lead to a sparseness of observations in certain situations.

Figure 9 shows the ΔXCH_4 vs. ΔXCO_2 measurements recorded over Sumatra, for the entire 2-month period (September–October) (top) and for Period 1 (middle) and Period 2 (bottom) only. Over the 2 months, a total of 66 fire-affected TANSO-FTS measurements are identified that have a suitable matching background available from which to calculate ΔXCH_4 and ΔXCO_2 . The linear best fit to these data give a $\text{CH}_4 / \text{CO}_2$ ER of $6.64 \text{ ppb ppm}^{-1}$ ($R = 0.893$) for these Sumatran fires. When examining the Periods 1 and 2 only, which Fig. 8 shows correspond to times of increased fire activity over the island, higher ERs of 8.1 and 8.8 ppb ppm^{-1} are derived ($R = 0.91$ and 0.92 , respectively). These higher $\text{CH}_4 / \text{CO}_2$ ERs are consistent with the region being characterised by a larger proportion of smouldering combustion, most likely of peatland, given the preponderance of that land cover in the fire-affected area (Fig. 2), resulting in enhanced CH_4 concentrations as already observed in Sect. 5.

Similar to Fig. 9, Fig. 10 shows the ΔXCH_4 and ΔXCO_2 retrievals for Kalimantan, plotted on a scatterplot from which

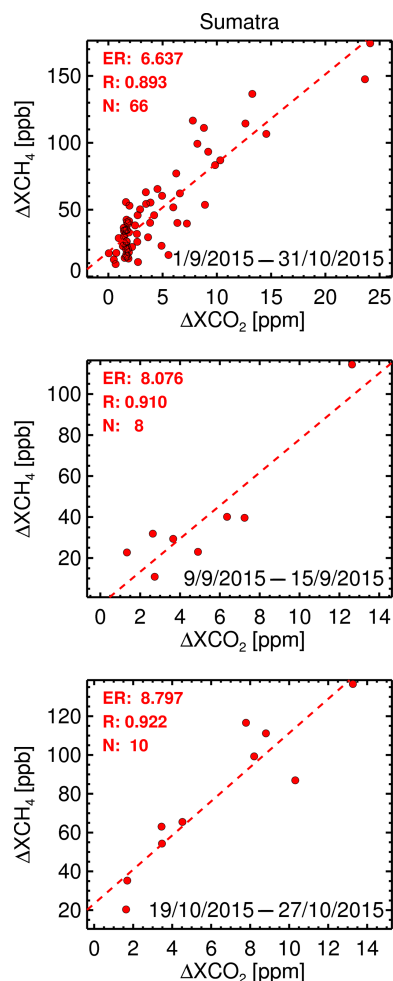


Figure 9. Scatterplots of ΔXCH_4 vs. ΔXCO_2 derived for Sumatran large-scale fire plumes via analysis of TANSO-FTS data for the time periods detailed in Fig. 8: September–October 2015 (top), Period 1: 9–15 September (middle) and Period 2: 19–27 October (bottom). The $\text{CH}_4 / \text{CO}_2$ ER is calculated as the gradient of a linear fit to the data (dashed line). The correlation coefficient R and the number of soundings N are also shown.

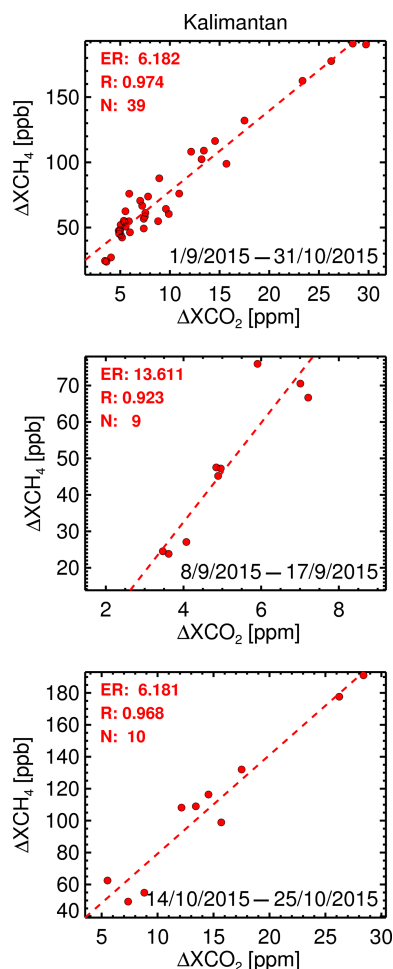


Figure 10. Scatterplots of $\Delta X\text{CH}_4$ vs. $\Delta X\text{CO}_2$ derived for Kalimantan large-scale fire plumes via analysis of TANSO-FTS data for the time periods detailed in Fig. 8: September–October 2015 (top), Period 1: 8–17 September (middle) and Period 2: 14–25 October (bottom). The CH_4/CO_2 ER is calculated as the gradient of a linear fit to the data (dashed line). The correlation coefficient R and the number of soundings N are also shown.

the CH_4/CO_2 ER can be derived. Over the 2 months of September and October 2015, Fig. 8 shows that Kalimantan appears characterised by typically lower amounts of fire activity than Sumatra, interspersed with relatively short but intense episodes, such as those on 8 September and 14 October. The CH_4/CO_2 ER calculated for the Kalimantan data across the entire 2-month period is found to be 6.2 ppb ppm^{-1} , calculated from 39 separate $\Delta X\text{CH}_4$ and $\Delta X\text{CO}_2$ observations (correlation coefficient of 0.974). However, when examining Period 1 only (8–17 September), although derived from only nine data points ($R = 0.92$) an extremely high ER is found ($13.6 \text{ ppb ppm}^{-1}$, $R = 0.92$). By contrast, during Period 2 (14–25 October) the ER is found once again to be lower, at 6.2 ppb ppm^{-1} ($R = 0.97$). This lower value may be affected by the fact that throughout Period 2 extensive smoke aerosol

covers much of Kalimantan (as seen in Fig. 4) and the selection of clear TANSO-FTS that appropriately represent the clean background of the fire-affected measurements is significantly more difficult. This is further compounded by the fact that the wind vectors (not shown) for this period indicate that the background air is likely to be coming from further south, potentially having a different CH_4 and CO_2 concentration.

6.1 Ground-based ERs from El Niño-enhanced peat and vegetation fires

In addition to space-based observations described above, during October 2015, at the height of the fire activity on Kalimantan (Fig. 8), a short field campaign was conducted to derive CH_4 to CO_2 ERs for comparison to the GOSAT-derived values. During this campaign, smoke was sampled and ERs derived for individual fire plumes stemming from the El Niño-enhanced landscape fires. Trace gas mixing ratio measures of CO_2 and CH_4 were made at 1 Hz frequency in plumes from fires at four different locations within $\sim 30 \text{ km}$ of Palangkaraya (2.21° S , 113.92° E), the capital of Central Kalimantan and one of the most fire-affected regions during the 2015 El Niño related drought (Drake, 2015). We use a ground-based, more portable version of the cavity-enhanced laser absorption spectrometer described in O’Shea et al. (2013). The precision (Allan variance, 1σ at 1 Hz) of the mixing ratios derived via the laser spectroscopy was 1.71 ppb for CH_4 and 2.63 ppm for CO_2 , with a total absolute uncertainty of around 1% of the measured concentrations. Fires at the four different locations were sampled between 12 and 16 October 2015, with each site located on peat but with plumes encompassing both pure peat burning and also times when both peat and some overlying vegetation were being consumed. The CH_4/CO_2 ERs determined from these close-to-source measurements varied between 7.53 and $19.7 \text{ ppb ppm}^{-1}$ (mean \pm sd = $12.9 \pm 3.9 \text{ ppb ppm}^{-1}$), a range relatively consistent with that determined from the GOSAT-derived, space-based observations (6.18 – $13.6 \text{ ppb ppm}^{-1}$). However, the majority of the ground-based ERs were derived from locations dominated by almost pure peat burning sampled close to the source, whereas the space-based observations from GOSAT are derived from measurements of the smoke filling a 10.5 km diameter TANSO-FTS footprint and thus representative of much larger areas of combustion, very likely comprising a mix of peat and vegetation burning in the majority of cases.

Despite this potential for the GOSAT-derived CH_4 to CO_2 ER to be somewhat less characteristic of pure peat burning than are some of the close-to-source measurements, and the potential for the measurements to be influenced by cleaner air (such as that transported from the south), it is still expected that the emissions over Indonesia will be largely dominated by smouldering combustion, resulting in a typically higher CH_4/CO_2 ER than that observed from flaming com-

bustion as is generally characteristic of most African savannah burning (Wooster et al., 2011). To confirm that this is the case, the same GOSAT-based analysis performed here for the 2015 Indonesian fires was also performed for southern Africa (defined as 0° N–40° S, 30° W–60° E) and the Amazon (defined as 0° N–40° S, 30–75° W), both of which underwent significant fire activity during this same time period. The calculated CH₄ / CO₂ ER for southern Africa was found to be 4.35 ppb ppm⁻¹ (see Appendix B, Fig. B1), consistent with observations of flaming-dominated combustion in savannah regions. Wooster et al. (2011), using a ground-based, open-path FTIR system, reported CH₄ to CO₂ ERs for different phases of southern African savannah burns conducted on 7 ha plots in Kruger National Park, South Africa. Backfires (spreading against the wind) typically produced emissions with very complete combustion characteristics, with CH₄ to CO₂ ERs of 1.9–2.2 ppb ppm⁻¹, apart from one case where a value of 6.0 ppb ppm⁻¹ was recorded. Residual areas of smouldering combustion present after the fire front had passed were recorded as having CH₄ to CO₂ ERs of 3.1–14.1 ppb ppm⁻¹, although it was possible that the lowest ERs reported were significantly influenced by remaining pockets of flaming activity. The headfire emissions, which combine the smoke from the most intense flaming part of the burn with those from the smouldering zone immediately behind, were found to have CH₄ to CO₂ ERs of 2.4–5.4 ppb ppm⁻¹. The overall fire-averaged CH₄ to CO₂ ER, calculated from the ERs of the individual phases and using airborne measures of FRP to estimate the amount the fuel consumption in each for the purposes of the weighting calculation, was 4.3 ± 1.7 ppb ppm⁻¹, very close to the 4.35 ppb ppm⁻¹ derived from GOSAT's observations of large-scale southern African savannah plumes. This provides further evidence for the representative nature of our GOSAT approach, which is currently the only method able to assess the ERs of the largest plumes emanating from landscape fires, albeit only at the relatively sparse sampling locations targeted by GOSAT. The CH₄ / CO₂ ER for the Amazon is, as perhaps expected, somewhat in between that of African savannah and Indonesian peatlands and forests, being 5.1 ppb ppm⁻¹ (see Fig. B2). Guild et al. (2004) and references therein report the presence of significant smouldering combustion in Amazon fires occurring in forested regions, much more than typically seen in African savannah and primarily stemming from the coarse woody fuels that represent a significant component of the fuel in this biome. However, smouldering in the peat-dominated fuels of the Indonesian fires would still be expected to be more prevalent (Stockwell et al., 2014), and so the CH₄ to CO₂ ER would be expected to be higher there, as we have indeed found.

7 Summary and outlook

The objective of this study was to utilise XCH₄ and XCO₂ observations made by the GOSAT satellite when passing over Indonesia to probe the composition of large-scale plumes from the 2015 Indonesian fires for the first time, with these extreme fires being driven by the ongoing strong El Niño, the largest seen since 1997–1998. We wished to both identify the atmospheric greenhouse gas impacts of the very significant increase in fire activity and use any such measurements to determine the biomass burning ERs of these two important GHGs using the technique we pioneered in Ross et al. (2013). This would enable the characterisation of certain aspects of the chemical makeup of these large-scale El Niño-driven fires for the first time, which, in 1997–1998, were responsible for the largest release of fire-emitted GHGs seen worldwide, and indeed which are believed to be of a magnitude not seen since that period anywhere on Earth (van der Werf et al., 2010).

Our analysis of GOSAT data confirms a significant enhancement of both XCH₄ and XCO₂ in the fire-affected GOSAT soundings, with the greatest change seen in the XCH₄ mixing ratios where we see an average value of 1840.1 ppb compared to an average value in the clear (non-fire-affected) cases of 1805.5 ppb. For these fire-affected soundings, the CH₄ / CO₂ ER was estimated from the gradient of the linear best fit to the excess XCH₄ and XCO₂ values. We find an overall ER for the entire Indonesian fire-affected region during the September–October 2015 fire peak of 6.2 ppb ppm⁻¹, with Sumatra showing slightly higher mean ERs (6.6 ppb ppm⁻¹) than Kalimantan (6.2 ppb ppm⁻¹). When examining shorter periods of time to focus on specific fire episodes on each island, we find ERs as low as 6.1 and as high as 13.6 ppb ppm⁻¹. This range is consistent with that seen in field-sampled GHG data taken in October 2015 on Kalimantan, close to the fire sources, but we believe the large-scale sampling provided by the GOSAT TANSO-FTS 10.5 km diameter footprints enables sampling of a much more representative amount of smoke than does the relatively limited, small-scale sampling possible on the ground. We therefore believe that our GOSAT-derived ERs are well suited for use in studies attempting to understand the impact of these extreme El Niño-driven fires on the larger-scale, regional atmosphere.

Our GOSAT-derived ERs for Indonesia indicate plumes that appear more dominated by the products of smouldering combustion than the plumes sampled by GOSAT in southern Africa and in the Amazon during the same period, consistent with prior expectation and previous ground-based and airborne sampling campaigns that suggest less smouldering-dominated combustion in these latter biomes (especially in the savannah case). GOSAT's capability to determine not only the enhancement in greenhouse gas abundance stemming from such large fire events but also to provide the data necessary to calculate the GHG emission ratios and help identify the relative balance of smouldering and flam-

ing activity ongoing in very large regions is an extremely valuable aid to understanding the composition of the plumes and their impact on regional atmospheric composition and climate. Some challenges remain, mainly relating to obtaining an accurate representation of the background non-fire-affected XCH_4 and XCO_2 amounts (see Appendix A). However, the technique that we present here and in Ross et al. (2013) should be easily applicable to future satellite missions focused on atmospheric composition. Several of these will have increased spatial and temporal resolutions that will greatly aid in obtaining the most suitable background observations. One such mission, Sentinel-5 Precursor, is planned for launch in 2016 and is capable of measuring both CH_4 and CO at a high spatial resolution, providing an ability that GOSAT currently lacks. We believe, therefore, that this work will prove valuable in eventually facilitating the routine determination of regional biomass burning ERs from space, and their spatiotemporal variations whose importance is described in, e.g. Van Leeuwen and Van Der Werf (2011). Such a capability might ultimately allow the characterisation of such burning events under different climatic and biome conditions.

8 Data availability

The University of Leicester Proxy XCH_4 data used in this work is available as part of the ESA GHG-CCI Project, freely available from <http://www.esa-ghg-cci.org>. Please contact Dr. Robert Parker for more details.

Appendix A

As discussed in Sect. 6, there exists the potential to introduce errors into the GOSAT-derived ERs if the fire-affected sounding and the background sounding each contain sufficiently different aerosol scattering characteristics. As the fire-affected sounding will, by definition, usually contain a non-trivial amount of smoke aerosols, whilst the background sounding is, in theory, supposed to be free of smoke, some quantification of this affect is needed. In this section, we derive and use a simple mathematical representation to determine the magnitude of such effects.

Let the observed excess concentration be the difference between the observed fire and background concentrations:

$$\Delta XCH_4 = XCH_4^{\text{fire}} - XCH_4^{\text{bgd}}. \quad (\text{A1})$$

Both soundings will have an error due to scattering associated with them, which typically lengthens the light path and hence reduces the inferred gas mixing ratio. This error factor, here termed A , will be different for the fire and background cases.

Therefore,

$$\Delta XCH_4 = A_{\text{fire}}XCH_4^{\text{fire}} - A_{\text{bgd}}XCH_4^{\text{bgd}}. \quad (\text{A2})$$

Similarly, for XCO_2 we have

$$\Delta XCO_2 = A_{\text{fire}}XCO_2^{\text{fire}} - A_{\text{bgd}}XCO_2^{\text{bgd}}. \quad (\text{A3})$$

The ratio of the excess concentrations due to the fire emissions, from which we calculate the CH_4 to CO_2 ER, is then given by

$$\frac{\Delta XCH_4}{\Delta XCO_2} = \frac{A_{\text{fire}}XCH_4^{\text{fire}} - A_{\text{bgd}}XCH_4^{\text{bgd}}}{A_{\text{fire}}XCO_2^{\text{fire}} - A_{\text{bgd}}XCO_2^{\text{bgd}}}. \quad (\text{A4})$$

Now, we set the observed CH_4 concentration in the fire sounding to the background concentration, plus the true excess concentration related to the fire:

$$XCH_4^{\text{fire}} = XCH_4^{\text{bgd}} + \Delta XCH_4^{\text{true}}. \quad (\text{A5})$$

Doing the same for XCO_2 now gives

$$\frac{\Delta XCH_4}{\Delta XCO_2} = \frac{A_{\text{fire}}(XCH_4^{\text{bgd}} + \Delta XCH_4^{\text{true}}) - A_{\text{bgd}}XCH_4^{\text{bgd}}}{A_{\text{fire}}(XCO_2^{\text{bgd}} + \Delta XCO_2^{\text{true}}) - A_{\text{bgd}}XCO_2^{\text{bgd}}}. \quad (\text{A6})$$

This can then be expanded to

$$\frac{\Delta XCH_4}{\Delta XCO_2} = \frac{A_{\text{fire}}XCH_4^{\text{bgd}} + A_{\text{fire}}\Delta XCH_4^{\text{true}} - A_{\text{bgd}}XCH_4^{\text{bgd}}}{A_{\text{fire}}XCO_2^{\text{bgd}} + A_{\text{fire}}\Delta XCO_2^{\text{true}} - A_{\text{bgd}}XCO_2^{\text{bgd}}}, \quad (\text{A7})$$

and then rearranged to

$$\frac{\Delta XCH_4}{\Delta XCO_2} = \frac{(A_{\text{fire}} - A_{\text{bgd}})XCH_4^{\text{bgd}} + A_{\text{fire}}\Delta XCH_4^{\text{true}}}{(A_{\text{fire}} - A_{\text{bgd}})XCO_2^{\text{bgd}} + A_{\text{fire}}\Delta XCO_2^{\text{true}}}. \quad (\text{A8})$$

Now, let the ratio of the two error terms be

$$A_{\text{ratio}} = A_{\text{fire}}/A_{\text{bgd}}, \quad (\text{A9})$$

which then rearranged gives

$$A_{\text{fire}} = A_{\text{ratio}}A_{\text{bgd}}. \quad (\text{A10})$$

Therefore,

$$A_{\text{fire}} - A_{\text{bgd}} = A_{\text{ratio}}A_{\text{bgd}} - A_{\text{bgd}} = A_{\text{bgd}}(A_{\text{ratio}} - 1). \quad (\text{A11})$$

Substituting this in now gives

$$\frac{\Delta XCH_4}{\Delta XCO_2} = \frac{(A_{\text{bgd}}(A_{\text{ratio}} - 1))XCH_4^{\text{bgd}} + A_{\text{ratio}}A_{\text{bgd}}\Delta XCH_4^{\text{true}}}{(A_{\text{bgd}}(A_{\text{ratio}} - 1))XCO_2^{\text{bgd}} + A_{\text{ratio}}A_{\text{bgd}}\Delta XCO_2^{\text{true}}}. \quad (\text{A12})$$

The A_{bgd} terms cancel, giving

$$\frac{\Delta XCH_4}{\Delta XCO_2} = \frac{(A_{\text{ratio}} - 1)XCH_4^{\text{bgd}} + A_{\text{ratio}}\Delta XCH_4^{\text{true}}}{(A_{\text{ratio}} - 1)XCO_2^{\text{bgd}} + A_{\text{ratio}}\Delta XCO_2^{\text{true}}}. \quad (\text{A13})$$

This equation therefore relates the observed excess concentrations (ΔXCH_4 and ΔXCO_2) calculated from the difference in GOSAT's fire-affected and background soundings to the true background concentrations (XCH_4^{bgd} and XCO_2^{bgd}), the true excess concentrations ($\Delta XCH_4^{\text{true}}$ and $\Delta XCO_2^{\text{true}}$) and the ratio between the error terms, A_{ratio} . Furthermore, we can use this simple relationship to explore the likely error in the calculated ER for a given value of A_{ratio} .

Figure A1 shows the implementation of Eq. (A13) for various scenarios. The background XCH_4 and XCO_2 concentrations are fixed at 1850 ppb and 400 ppm, respectively, representing the normal fire-free atmosphere. The true methane enhancement ($\Delta XCH_4^{\text{true}}$) is varied between 0 and 50 ppb in 5 ppb increments and the true ER between CH_4 and CO_2 is varied between 0.003 and 0.012. The different panels then show the behaviour for various ranges of A_{ratio} . The top left panel has A_{ratio} set at a constant value of 1 (i.e. the error in

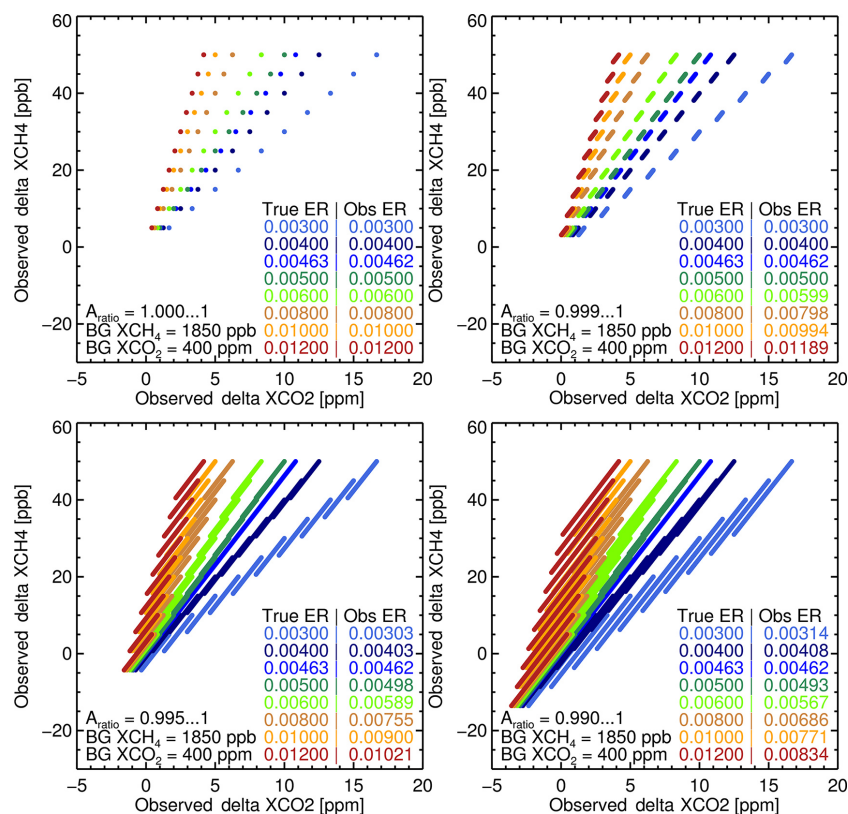


Figure A1. Implementation of Eq. (A13) with ΔXCH_4 varied between 5 and 50 ppb for ERs ranging from 0.003 to 0.009 for different ranges of A_{ratio} . The true ERs and the ERs derived from the observed correlation are shown in each panel. The top left figure shows a fixed value of $A_{\text{ratio}} = 1$ while the remaining panels (clockwise) show the value of A_{ratio} ranging from 0.999 to 1, 0.99 to 1 and 0.995 to 1.

the background is exactly the same as the error in the fire cases), which is the ideal situation, and the true ERs are reproduced exactly. The top right panel allows A_{ratio} to vary between 0.999 and 1.0. The effect of this is a slight spreading of the lines and the difference between the true and observed ER is minimal. The bottom left panel shows the increased range of A_{ratio} from 0.995 to 1.0, which causes the observed ERs to differ more from the truth, with a true ER of 0.008 only appearing as an observed ratio of 0.00755, an error of 5.6%. Finally, in the bottom right panel, the value of A_{ratio} is allowed to vary between 0.99 and 1.0. This relatively large variation decreases the observed ER further, with a true ER of 0.008 appearing as an observed ratio of 0.00686, for example.

Whilst there are many unknowns that impact the value of A_{ratio} , and so it is not possible to know its exact value for a particular pair of GOSAT fire-affected and background observations used to derive an emission ratio, it is possible to determine its expected range. By comparing the scatter of the fire-affected and background XCH₄ values to the Proxy XCH₄ data (which are much less affected by aerosol and in this case used as the truth) it is possible to estimate the likely range of values of A_{ratio} . The standard deviation of the ratio between the XCH₄ / Proxy XCH₄ for the background and

fire cases is found to be 0.00494, suggesting that values of A_{ratio} are likely in the 0.995–1.0 range (i.e. up to a 0.5% reduction in A). This means that whilst we are likely to tend to underestimate the true CH₄ to CO₂ emission ratios with GOSAT, for the majority of cases (CH₄ to CO₂ ERs in the range 0.005–0.008) the effect can be considered small, with typical biases of 0.4–5.6%. Even in extreme cases with high ERs (e.g. 0.012), we expect an error of less than 15%.

Appendix B

This section contains ΔXCH_4 vs. ΔXCO_2 correlation plots for southern Africa (Fig. B1) and the Amazon (Fig. B2), as discussed in the main text in Sect. 6.

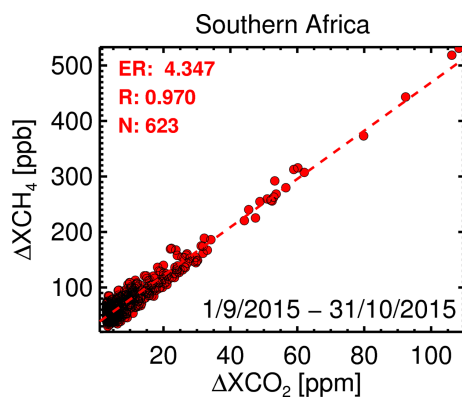


Figure B1. Scatterplot showing the $\Delta X\text{CH}_4$ vs. $\Delta X\text{CO}_2$ values, calculated as the difference between the values in the fire-affected soundings to those in the background cases over the entire southern African region from 1 September to 31 October 2015. The CH_4/CO_2 ER is calculated from the gradient of the linear best fit, which is shown along with the correlation coefficient R and the number of sounding pairs N . This GOSAT-derived ER is very similar to the fire-averaged CH_4 to CO_2 ER of 4.3 ± 1.7 ppb ppm⁻¹ derived by Wooster et al. (2011) using open-path FTIR spectroscopy measurements close to the source on these types of savannah fire events.

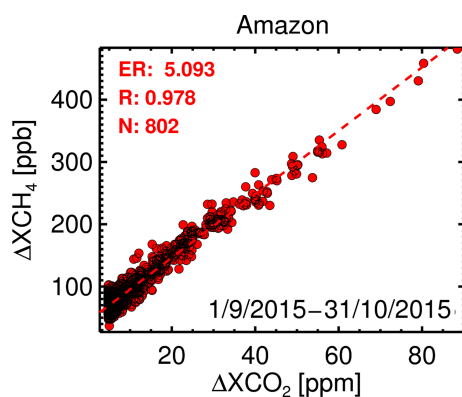


Figure B2. Scatterplot showing the $\Delta X\text{CH}_4$ vs. $\Delta X\text{CO}_2$ values, calculated as the difference between the values in the fire-affected soundings to those in the background cases over the entire Amazonian region from 1 September to 31 October 2015. The CH_4/CO_2 ER is calculated from the gradient of a linear fit to the data. This line of best fit is also shown, along with the correlation coefficient R and the number of soundings N .

Acknowledgements. R. J. Parker is funded via an ESA Living Planet Fellowship with additional funding from the UK National Centre for Earth Observation (NCEO) and the ESA Greenhouse Gas Climate Change Initiative (GHG-CCI). H. Boesch, D. Moore and M. Wooster are also supported by NERC NCEO. A. J. Webb is funded by a NERC PhD. Field measurements in Indonesia were part supported by NERC grant NE/J010502/1 (NERC SAMBBA). Field measurements were also part supported by a DFID grant to CIFOR (project no. 203034). Bruce Main at King's College London and Agus Salim at CIFOR are thanked for their technical contributions to the field measurement campaign. D. Murdiyarso acknowledges the support provided by USAID and USFS. This work also relates to NERC grant NE/N01555X/1.

We thank the Japanese Aerospace Exploration Agency, National Institute for Environmental Studies, and the Ministry of Environment for the GOSAT data and their continuous support as part of the Joint Research Agreement. We also thank CAMS for provision of the data from GFAS. We also acknowledge the use of MODIS Active Fire Detections extracted from MCD14ML distributed by NASA FIRMS (available on-line at <https://earthdata.nasa.gov/active-fire-data>). We thank EUMETSAT for the IASI CO Level 2 data. IASI is a joint mission of EUMETSAT and the Centre National d'études Spatiales (CNES, France).

Finally, this research used the ALICE High Performance Computing Facility at the University of Leicester.

Edited by: M. Chipperfield

Reviewed by: two anonymous referees

References

- Alexe, M., Bergamaschi, P., Segers, A., Detmers, R., Butz, A., Hasekamp, O., Guerlet, S., Parker, R., Boesch, H., Frankenberg, C., Scheepmaker, R. A., Dlugokencky, E., Sweeney, C., Wofsy, S. C., and Kort, E. A.: Inverse modelling of CH₄ emissions for 2010–2011 using different satellite retrieval products from GOSAT and SCIAMACHY, *Atmos. Chem. Phys.*, 15, 113–133, doi:10.5194/acp-15-113-2015, 2015.
- Andreae, M. O. and Merlet, P.: Emission of trace gases and aerosols from biomass burning, *Global Biogeochem. Cy.*, 15, 955–966, doi:10.1029/2000GB001382, 2001.
- Bertschi, I. T., Yokelson, R. J., Ward, D. E., Christian, T. J., and Hao, W. M.: Trace gas emissions from the production and use of domestic biofuels in Zambia measured by open-path Fourier transform infrared spectroscopy, *J. Geophys. Res.-Atmos.*, 108, D13, doi:10.1029/2002JD002158, 2003.
- Boesch, H., Baker, D., Connor, B., Crisp, D., and Miller, C.: Global Characterization of CO₂ Column Retrievals from Shortwave-Infrared Satellite Observations of the Orbiting Carbon Observatory-2 Mission, *Remote Sensing*, 3, 270–304, doi:10.3390/rs3020270, 2011.
- Bonsang, B., Boissard, C., Le Cloarec, M., Rudolph, J., and La-caux, J.: Methane, carbon monoxide and light non-methane hydrocarbon emissions from African savanna burnings during the FOS/DECAFE experiment, *J. Atmos. Chem.*, 22, 149–162, doi:10.1007/BF00708186, 1995.
- Buchwitz, M., Reuter, M., Schneising, O., Boesch, H., Guerlet, S., Dils, B., Aben, I., Armante, R., Bergamaschi, P., Blumenstock, T., Bovensmann, H., Brunner, D., Buchmann, B., Burrows, J., Butz, A., Chadin, A., Chevallier, F., Crevoisier, C., Deutscher, N., Frankenberg, C., Hase, F., Hasekamp, O., Heymann, J., Kaminski, T., Laeng, A., Lichtenberg, G., Maziere, M. D., Noel, S., Notholt, J., Orphal, J., Popp, C., Parker, R., Scholze, M., Sussmann, R., Stiller, G., Warneke, T., Zehner, C., Bril, A., Crisp, D., Griffith, D., Kuze, A., O'Dell, C., Oshchepkov, S., Sherlock, V., Suto, H., Wennberg, P., Wunch, D., Yokota, T., and Yoshida, Y.: The Greenhouse Gas Climate Change Initiative (GHG-CCI): Comparison and quality assessment of near-surface-sensitive satellite-derived {CO₂} and {CH₄} global data sets, *Remote Sens. Environ.*, 162, 344–362, doi:10.1016/j.rse.2013.04.024, 2015.
- Butz, A., Hasekamp, O. P., Frankenberg, C., Vidot, J., and Aben, I.: CH₄ retrievals from space-based solar backscatter measurements: Performance evaluation against simulated aerosol and cirrus loaded scenes, *J. Geophys. Res.-Atmos.*, 115, D21, doi:10.1029/2010JD014514, 2010.
- CAMS-GFAS, E.: CAMS Global Fire Assimilation System, available at: <http://apps.ecmwf.int/datasets/data/cams-gfas/> (last access: 1 August 2016), 2016.
- Christian, T. J., Kleiss, B., Yokelson, R. J., Holzinger, R., Crutzen, P. J., Hao, W. M., Saharjo, B. H., and Ward, D. E.: Comprehensive laboratory measurements of biomass-burning emissions: 1. Emissions from Indonesian, African, and other fuels, *J. Geophys. Res.-Atmos.*, 108, 4719, doi:10.1029/2003JD003704, 2003.
- Christian, T. J., Yokelson, R. J., Carvalho, J. A., Griffith, D. W. T., Alvarado, E. C., Santos, J. C., Neto, T. G. S., Veras, C. A. G., and Hao, W. M.: The tropical forest and fire emissions experiment: Trace gases emitted by smoldering logs and dung from deforestation and pasture fires in Brazil, *J. Geophys. Res.-Atmos.*, 112, d18308, doi:10.1029/2006JD008147, 2007.
- Cofer, W. R., Winstead, E. L., Stocks, B. J., Goldammer, J. G., and Cahoon, D. R.: Crown fire emissions of CO₂, CO, H₂, CH₄, and TNMHC from a dense Jack pine boreal forest fire, *Geophys. Res. Lett.*, 25, 3919–3922, doi:10.1029/1998GL900042, 1998.
- Cogan, A., Boesch, H., Parker, R., Feng, L., Palmer, P., Blavier, J.-F., Deutscher, N. M., Macatangay, R., Notholt, J., Roehl, C., Warneke, T., and Wunch, D.: Atmospheric carbon dioxide retrieved from the Greenhouse gases Observing SATellite (GOSAT): Comparison with ground-based TCCON observations and GEOS-Chem model calculations, *J. Geophys. Res.-Atmos.*, 117, D21, doi:10.1029/2012JD018087, 2012.
- Coheur, P.-F., Clarisse, L., Turquety, S., Hurtmans, D., and Clerbaux, C.: IASI measurements of reactive trace species in biomass burning plumes, *Atmos. Chem. Phys.*, 9, 5655–5667, doi:10.5194/acp-9-5655-2009, 2009.
- Cressot, C., Chevallier, F., Bousquet, P., Crevoisier, C., Dlugokencky, E. J., Fortems-Cheiney, A., Frankenberg, C., Parker, R., Pison, I., Scheepmaker, R. A., Montzka, S. A., Krummel, P. B., Steele, L. P., and Langenfelds, R. L.: On the consistency between global and regional methane emissions inferred from SCIAMACHY, TANSO-FTS, IASI and surface measurements, *Atmos. Chem. Phys.*, 14, 577–592, doi:10.5194/acp-14-577-2014, 2014.
- Drake, N.: Indonesia blazes threaten endangered orangutans, *Nature*, 527, 18, doi:10.1038/527018a, 2015.
- Frankenberg, C., Meirink, J. F., Bergamaschi, P., Goede, A. P. H., Heimann, M., Körner, S., Platt, U., van Weele, M., and Wagner, T.: Satellite cartography of atmospheric methane

- from SCIAMACHY on board ENVISAT: Analysis of the years 2003 and 2004, *J. Geophys. Res.-Atmos.*, 111, d07303, doi:10.1029/2005JD006235, 2006.
- Fraser, A., Palmer, P. I., Feng, L., Boesch, H., Cogan, A., Parker, R., Dlugokencky, E. J., Fraser, P. J., Krummel, P. B., Langenfelds, R. L., O'Doherty, S., Prinn, R. G., Steele, L. P., van der Schoot, M., and Weiss, R. F.: Estimating regional methane surface fluxes: the relative importance of surface and GOSAT mole fraction measurements, *Atmos. Chem. Phys.*, 13, 5697–5713, doi:10.5194/acp-13-5697-2013, 2013.
- Fraser, A., Palmer, P. I., Feng, L., Bösch, H., Parker, R., Dlugokencky, E. J., Krummel, P. B., and Langenfelds, R. L.: Estimating regional fluxes of CO₂ and CH₄ using space-borne observations of XCH₄: XCO₂, *Atmos. Chem. Phys.*, 14, 12883–12895, doi:10.5194/acp-14-12883-2014, 2014.
- Freeborn, P. H., Wooster, M. J., Hao, W. M., Ryan, C. A., Nordgren, B. L., Baker, S. P., and Ichoku, C.: Relationships between energy release, fuel mass loss, and trace gas and aerosol emissions during laboratory biomass fires, *J. Geophys. Res.-Atmos.*, 113, D1, doi:10.1029/2007JD008679, 2008.
- Gaveau, D. L., Salim, M. A., Hergoualc'h, K., Locatelli, B., Sloan, S., Wooster, M., Marlier, M. E., Molidena, E., Yaen, H., DeFries, R., Verchot, L., Murdiyarso, D., Nasi, R., Holmgren, P., and Sheil, D.: Major atmospheric emissions from peat fires in Southeast Asia during non-drought years: evidence from the 2013 Sumatran fires, *Scientific reports*, 4, 6112, doi:10.1038/srep06112, 2014.
- Giglio, L., Descloitres, J., Justice, C. O., and Kaufman, Y. J.: An enhanced contextual fire detection algorithm for MODIS, *Remote Sens. Environ.*, 87, 273–282, doi:10.1016/S0034-4257(03)00184-6, 2003.
- Guild, L. S., Kauffman, J. B., Cohen, W. B., Hlavka, C. A., and Ward, D. E.: Modeling biomass burning emissions for amazon forest and pastures in Rondônia, Brazil, *Ecol. Appl.*, 14, 232–246, doi:10.1890/01-6009, 2004.
- Hartmann, D., Klein Tank, A., Rusticucci, M., Alexander, L., Brönnimann, S., Charabi, Y., Dentener, F., Dlugokencky, E., Easterling, D., Kaplan, A., Soden, B., Thorne, P., Wild, M., and Zhai, P.: Observations: Atmosphere and Surface, book section 2, Cambridge University Press, Cambridge, United Kingdom and New York, NY, USA, 159–254, doi:10.1017/CBO9781107415324.008, 2013.
- Huijnen, V., Wooster, M. J., Kaiser, J. W., Gaveau, D. L. A., Fleming, J., Parrington, M., Inness, A., Murdiyarso, D., Main, B., and van Weele, M.: Fire carbon emissions over maritime southeast Asia in 2015 largest since 1997, *Scientific Reports*, 6, 26886, doi:10.1038/srep26886, 2016.
- Hurst, D. F., Griffith, D. W., and Cook, G. D.: Trace gas emissions from biomass burning in tropical Australian savannas, *J. Geophys. Res.-Atmos.*, 99, 16441–16456, doi:10.1029/94JD00670, 1994.
- Inness, A., Blechschmidt, A.-M., Bouarar, I., Chabrilat, S., Crepulja, M., Engelen, R. J., Eskes, H., Flemming, J., Gaudel, A., Hendrick, F., Huijnen, V., Jones, L., Kapsomenakis, J., Katragkou, E., Keppens, A., Langerock, B., de Mazière, M., Melas, D., Parrington, M., Peuch, V. H., Razinger, M., Richter, A., Schultz, M. G., Suttie, M., Thouret, V., Vrekoussis, M., Wagner, A., and Zerefos, C.: Data assimilation of satellite-retrieved ozone, carbon monoxide and nitrogen dioxide with ECMWF's Composition-IFS, *Atmos. Chem. Phys.*, 15, 5275–5303, doi:10.5194/acp-15-5275-2015, 2015.
- Kaiser, J. W., Heil, A., Andreae, M. O., Benedetti, A., Chubarova, N., Jones, L., Morcrette, J.-J., Razinger, M., Schultz, M. G., Suttie, M., and van der Werf, G. R.: Biomass burning emissions estimated with a global fire assimilation system based on observed fire radiative power, *Biogeosciences*, 9, 527–554, doi:10.5194/bg-9-527-2012, 2012.
- Kasischke, E. S. and Bruhwiler, L. P.: Emissions of carbon dioxide, carbon monoxide, and methane from boreal forest fires in 1998, *J. Geophys. Res.-Atmos.*, 107, 8146, doi:10.1029/2001JD000461, 2002.
- Koppmann, R., Khedim, A., Rudolph, J., Poppe, D., Andreae, M. O., Helas, G., Welling, M., and Zenker, T.: Emissions of organic trace gases from savanna fires in southern Africa during the 1992 Southern African Fire Atmosphere Research Initiative and their impact on the formation of tropospheric ozone, *J. Geophys. Res.-Atmos.*, 102, 18879–18888, doi:10.1029/97JD00845, 1997.
- Koppmann, R., von Czapiewski, K., and Reid, J. S.: A review of biomass burning emissions, part I: gaseous emissions of carbon monoxide, methane, volatile organic compounds, and nitrogen containing compounds, *Atmos. Chem. Phys. Discuss.*, 5, 10455–10516, doi:10.5194/acpd-5-10455-2005, 2005.
- Korontzi, S., Ward, D. E., Susott, R. A., Yokelson, R. J., Justice, C. O., Hobbs, P. V., Smithwick, E. A. H., and Hao, W. M.: Seasonal variation and ecosystem dependence of emission factors for selected trace gases and PM_{2.5} for southern African savanna fires, *J. Geophys. Res.-Atmos.*, 108, 4758, doi:10.1029/2003JD003730, 2003.
- Kuze, A., Suto, H., Nakajima, M., and Hamazaki, T.: Thermal and near infrared sensor for carbon observation Fourier-transform spectrometer on the Greenhouse Gases Observing Satellite for greenhouse gases monitoring, *Appl. Opt.*, 48, 6716–6733, doi:10.1364/AO.48.006716, 2009.
- Kuze, A., Suto, H., Shiomi, K., Kawakami, S., Tanaka, M., Ueda, Y., Deguchi, A., Yoshida, J., Yamamoto, Y., Kataoka, F., Taylor, T. E., and Buijs, H. L.: Update on GOSAT TANSO-FTS performance, operations, and data products after more than 6 years in space, *Atmos. Meas. Tech.*, 9, 2445–2461, doi:10.5194/amt-9-2445-2016, 2016.
- Langner, A. and Siegert, F.: Spatiotemporal fire occurrence in Borneo over a period of 10 years, *Glob. Change Biol.*, 15, 48–62, doi:10.1111/j.1365-2486.2008.01828.x, 2009.
- Langner, A., Miettinen, J., and Siegert, F.: Land cover change 2002–2005 in Borneo and the role of fire derived from MODIS imagery, *Glob. Change Biol.*, 13, 2329–2340, doi:10.1111/j.1365-2486.2007.01442.x, 2007.
- Lee, T., Sullivan, A. P., Mack, L., Jimenez, J. L., Kreidenweis, S. M., Onasch, T. B., Worsnop, D. R., Malm, W., Wold, C. E., Hao, W. M., and Collett Jr., J. L.: Chemical Smoke Marker Emissions During Flaming and Smoldering Phases of Laboratory Open Burning of Wildland Fuels, *Aerosol Sci. Tech.*, 44, i–v, doi:10.1080/02786826.2010.499884, 2010.
- Liu, D., Allan, J. D., Young, D. E., Coe, H., Beddows, D., Fleming, Z. L., Flynn, M. J., Gallagher, M. W., Harrison, R. M., Lee, J., Prevot, A. S. H., Taylor, J. W., Yin, J., Williams, P. I., and Zotter, P.: Size distribution, mixing state and source apportionment of black carbon aerosol in London during winter-

- time, *Atmos. Chem. Phys.*, 14, 10061–10084, doi:10.5194/acp-14-10061-2014, 2014.
- Lober, J. M. and Warnatz, J.: Emissions from the combustion process in vegetation, in: *Fire in the Environment: The Ecological, Atmospheric and Climatic Importance of Vegetation Fires*, edited by: Crutzen, P. J. and Goldammer, J. G., John Wiley, 15–37, 1993.
- Myhre, G., Shindell, D., Bréon, F.-M., Collins, W., Fuglestedt, J., Huang, J., Koch, D., Lamarque, J.-F., Lee, D., Mendoza, B., Nakajima, T., Robock, A., Stephens, G., Takemura, T., and Zhang, H.: Anthropogenic and Natural Radiative Forcing, in: *Climate Change 2013: The Physical Science Basis. Contribution of Working Group I to the Fifth Assessment Report of the Intergovernmental Panel on Climate Change*, edited by: Stocker, T., Qin, D., Plattner, G.-K., Tignor, M., Allen, S., Boschung, J., Nauels, A., Xia, Y., Bex, V., and Midgley, P., Cambridge University Press, chapt. 8, 659–740, doi:10.1017/CBO9781107415324.018, 2013.
- O'Dell, C. W., Connor, B., Bösch, H., O'Brien, D., Frankenberg, C., Castano, R., Christi, M., Eldering, D., Fisher, B., Gunson, M., McDuffie, J., Miller, C. E., Natraj, V., Oyafuso, F., Polonsky, I., Smyth, M., Taylor, T., Toon, G. C., Wennberg, P. O., and Wunch, D.: The ACOS CO₂ retrieval algorithm – Part 1: Description and validation against synthetic observations, *Atmos. Meas. Tech.*, 5, 99–121, doi:10.5194/amt-5-99-2012, 2012.
- O'Shea, S. J., Bauguutte, S. J.-B., Gallagher, M. W., Lowry, D., and Percival, C. J.: Development of a cavity-enhanced absorption spectrometer for airborne measurements of CH₄ and CO₂, *Atmos. Meas. Tech.*, 6, 1095–1109, doi:10.5194/amt-6-1095-2013, 2013.
- Othman, M. and Latif, M.: Dust and gas emissions from small-scale peat combustion, *Aerosol Air Qual. Res.*, 13, 1045–1059, doi:10.4209/aaqr.2012.08.0214, 2013.
- Page, S. E., Siegert, F., Rieley, J. O., Boehm, H.-D. V., Jaya, A., and Limin, S.: The amount of carbon released from peat and forest fires in Indonesia during 1997, *Nature*, 420, 61–65, doi:10.1038/nature01131, 2002.
- Parker, R., Boesch, H., Cogan, A., Fraser, A., Feng, L., Palmer, P. I., Messerschmidt, J., Deutscher, N., Griffith, D. W., Notholt, J., Wennberg, P. O., and Wunch, D.: Methane observations from the Greenhouse Gases Observing SATellite: Comparison to ground-based TCCON data and model calculations, *Geophys. Res. Lett.*, 38, 15, doi:10.1029/2011GL047871, 2011.
- Parker, R. J., Boesch, H., Byckling, K., Webb, A. J., Palmer, P. I., Feng, L., Bergamaschi, P., Chevallier, F., Notholt, J., Deutscher, N., Warneke, T., Hase, F., Sussmann, R., Kawakami, S., Kivi, R., Griffith, D. W. T., and Velazco, V.: Assessing 5 years of GOSAT Proxy XCH₄ data and associated uncertainties, *Atmos. Meas. Tech.*, 8, 4785–4801, doi:10.5194/amt-8-4785-2015, 2015.
- Reid, J. S., Koppmann, R., Eck, T. F., and Eleuterio, D. P.: A review of biomass burning emissions part II: intensive physical properties of biomass burning particles, *Atmos. Chem. Phys.*, 5, 799–825, doi:10.5194/acp-5-799-2005, 2005.
- Ritung, S., Wahyunto, and Nugroho, K.: Peatland map of Indonesia, Office of Research and Development of Land Resources, Ministry of Agriculture, available at: <http://www.litbang.pertanian.go.id/unker/one/600/> (last access: 1 August 2016), 2016.
- Ross, A. N., Wooster, M. J., Boesch, H., and Parker, R.: First satellite measurements of carbon dioxide and methane emission ratios in wildfire plumes, *Geophys. Res. Lett.*, 40, 4098–4102, doi:10.1002/grl.50733, 2013.
- Schepers, D., Guerlet, S., Butz, A., Landgraf, J., Frankenberg, C., Hasekamp, O., Blavier, J.-F., Deutscher, N. M., Griffith, D. W. T., Hase, F., Kyro, E., Morino, I., Sherlock, V., Sussmann, R., and Aben, I.: Methane retrievals from Greenhouse Gases Observing Satellite (GOSAT) shortwave infrared measurements: Performance comparison of proxy and physics retrieval algorithms, *J. Geophys. Res.-Atmos.*, 117, D10, doi:10.1029/2012JD017549, 2012.
- Schroeder, W., Oliva, P., Giglio, L., and Csiszar, I. A.: The New {VIIRS} 375 m active fire detection data product: Algorithm description and initial assessment, *Remote Sens. Environ.*, 143, 85–96, doi:10.1016/j.rse.2013.12.008, 2014.
- Simmonds, P., Manning, A., Derwent, R., Ciais, P., Ramonet, M., Kazan, V., and Ryall, D.: A burning question. Can recent growth rate anomalies in the greenhouse gases be attributed to large-scale biomass burning events?, *Atmos. Environ.*, 39, 2513–2517, doi:10.1016/j.atmosenv.2005.02.018, 2005.
- Stockwell, C. E., Yokelson, R. J., Kreidenweis, S. M., Robinson, A. L., DeMott, P. J., Sullivan, R. C., Reardon, J., Ryan, K. C., Griffith, D. W. T., and Stevens, L.: Trace gas emissions from combustion of peat, crop residue, domestic biofuels, grasses, and other fuels: configuration and Fourier transform infrared (FTIR) component of the fourth Fire Lab at Missoula Experiment (FLAME-4), *Atmos. Chem. Phys.*, 14, 9727–9754, doi:10.5194/acp-14-9727-2014, 2014.
- Trenberth, K. E.: The Definition of El Niño, *B. Am. Meteorol. Soc.*, 78, 2771–2777, doi:10.1175/1520-0477(1997)078<2771:TDOENO>2.0.CO;2, 1997.
- Trigg, S. N., Curran, L. M., and McDonald, A. K.: Utility of Landsat 7 satellite data for continued monitoring of forest cover change in protected areas in Southeast Asia, *Singapore J. Trop. Geo.*, 27, 49–66, doi:10.1111/j.1467-9493.2006.00239.x, 2006.
- Turner, A. J., Jacob, D. J., Wecht, K. J., Maasakkers, J. D., Lundgren, E., Andrews, A. E., Biraud, S. C., Boesch, H., Bowman, K. W., Deutscher, N. M., Dubey, M. K., Griffith, D. W. T., Hase, F., Kuze, A., Notholt, J., Ohyama, H., Parker, R., Payne, V. H., Sussmann, R., Sweeney, C., Velazco, V. A., Warneke, T., Wennberg, P. O., and Wunch, D.: Estimating global and North American methane emissions with high spatial resolution using GOSAT satellite data, *Atmos. Chem. Phys.*, 15, 7049–7069, doi:10.5194/acp-15-7049-2015, 2015.
- van der Werf, G. R., Randerson, J. T., Collatz, G. J., Giglio, L., Kasibhatla, P. S., Arellano, A. F., Olsen, S. C., and Kasischke, E. S.: Continental-Scale Partitioning of Fire Emissions During the 1997 to 2001 El Niño/La Niña Period, *Science*, 303, 73–76, doi:10.1126/science.1090753, 2004.
- van der Werf, G. R., Dempewolf, J., Trigg, S. N., Randerson, J. T., Kasibhatla, P. S., Giglio, L., Murdiyarto, D., Peters, W., Morton, D. C., Collatz, G. J., Dolman, A. J., and DeFries, R. S.: Climate regulation of fire emissions and deforestation in equatorial Asia, *Proc. Natl. Acad. Sci.*, 105, 20350–20355, doi:10.1073/pnas.0803375105, 2008.
- van der Werf, G. R., Randerson, J. T., Giglio, L., Collatz, G. J., Mu, M., Kasibhatla, P. S., Morton, D. C., DeFries, R. S., Jin, Y., and van Leeuwen, T. T.: Global fire emissions and the contribution of deforestation, savanna, forest, agricultural, and peat fires (1997–

- 2009), *Atmos. Chem. Phys.*, 10, 11707–11735, doi:10.5194/acp-10-11707-2010, 2010.
- van Leeuwen, T. T. and van der Werf, G. R.: Spatial and temporal variability in the ratio of trace gases emitted from biomass burning, *Atmos. Chem. Phys.*, 11, 3611–3629, doi:10.5194/acp-11-3611-2011, 2011.
- Voiland, A.: Seeing Through the Smoky Pall: Observations from a Grim Indonesian Fire Season, available at: <http://earthobservatory.nasa.gov/Features/IndonesianFires> (last access: 1 August 2016), 2016.
- Wang, W., Ciais, P., Nemani, R. R., Canadell, J. G., Piao, S., Sitch, S., White, M. A., Hashimoto, H., Milesi, C., and Myneni, R. B.: Variations in atmospheric CO₂ growth rates coupled with tropical temperature, *Proc. Natl. Acad. Sci. USA*, 110, 13061–13066, doi:10.1073/pnas.1219683110, 2013.
- Wecht, K. J., Jacob, D. J., Sulprizio, M. P., Santoni, G. W., Wofsy, S. C., Parker, R., Bösch, H., and Worden, J.: Spatially resolving methane emissions in California: constraints from the CalNex aircraft campaign and from present (GOSAT, TES) and future (TROPOMI, geostationary) satellite observations, *Atmos. Chem. Phys.*, 14, 8173–8184, doi:10.5194/acp-14-8173-2014, 2014.
- Wolter, K.: Multivariate ENSO Index (MEI), available at: <http://www.esrl.noaa.gov/psd/enso/mei/>, last access: 1 August 2016.
- Wolter, K. and Timlin, M. S.: Measuring the strength of ENSO events: How does 1997/98 rank?, *Weather*, 53, 315–324, doi:10.1002/j.1477-8696.1998.tb06408.x, 1998.
- Wooster, M. and Zhang, Y.: Boreal forest fires burn less intensely in Russia than in North America, *Geophys. Res. Lett.*, 31, 20, doi:10.1029/2004GL020805, 2004.
- Wooster, M. J., Freeborn, P. H., Archibald, S., Oppenheimer, C., Roberts, G. J., Smith, T. E. L., Govender, N., Burton, M., and Palumbo, I.: Field determination of biomass burning emission ratios and factors via open-path FTIR spectroscopy and fire radiative power assessment: headfire, backfire and residual smouldering combustion in African savannahs, *Atmos. Chem. Phys.*, 11, 11591–11615, doi:10.5194/acp-11-11591-2011, 2011.
- Wooster, M. J., Ceccato, P., and Flasse, S. P.: Cover – Indonesian fires observed using AVHRR, *Int. J. Remote Sens.*, 19, 383–386, doi:10.1080/014311698216035, 1998.
- Wooster, M. J., Roberts, G., Perry, G. L. W., and Kaufman, Y. J.: Retrieval of biomass combustion rates and totals from fire radiative power observations: FRP derivation and calibration relationships between biomass consumption and fire radiative energy release, *J. Geophys. Res.-Atmos.*, 110, d24311, doi:10.1029/2005JD006318, 2005.
- Wooster, M. J., Perry, G. L. W., and Zoumas, A.: Fire, drought and El Niño relationships on Borneo (Southeast Asia) in the pre-MODIS era (1980–2000), *Biogeosciences*, 9, 317–340, doi:10.5194/bg-9-317-2012, 2012.
- Yokelson, R. J., Griffith, D. W. T., and Ward, D. E.: Open-path Fourier transform infrared studies of large-scale laboratory biomass fires, *J. Geophys. Res.-Atmos.*, 101, 21067–21080, doi:10.1029/96JD01800, 1996.
- Yokelson, R. J., Goode, J. G., Ward, D. E., Susott, R. A., Babbitt, R. E., Wade, D. D., Bertschi, I., Griffith, D. W., and Hao, W. M.: Emissions of formaldehyde, acetic acid, methanol, and other trace gases from biomass fires in North Carolina measured by airborne Fourier transform infrared spectroscopy, *J. Geophys. Res.-Atmos.*, 104, 30109–30125, doi:10.1029/1999JD900817, 1999.
- Yokelson, R. J., Christian, T. J., Karl, T. G., and Guenther, A.: The tropical forest and fire emissions experiment: laboratory fire measurements and synthesis of campaign data, *Atmos. Chem. Phys.*, 8, 3509–3527, doi:10.5194/acp-8-3509-2008, 2008.
- Yokelson, R. J., Andreae, M. O., and Akagi, S. K.: Pitfalls with the use of enhancement ratios or normalized excess mixing ratios measured in plumes to characterize pollution sources and aging, *Atmos. Meas. Tech.*, 6, 2155–2158, doi:10.5194/amt-6-2155-2013, 2013.